A high-Arctic inner shelf–fjord system from the Last Glacial Maximum to the Present: Bessel Fjord and SW Dove Bugt, NE Greenland

Authors: Kevin Zoller[1]; Jan Sverre Laberg[1]; Tom Arne Rydningen[1], Katrine Husum[2] & Matthias Forwick[1]

[1]Department of Geosciences, UiT The Arctic University of Norway, Box 6050 Langnes, NO-9037 Tromsø, Norway [2]Norwegian Polar Institute, Box 6606 Langnes, NO-9296 Tromsø, Norway

Correspondence to: Kevin Zoller (kevin.zoller3@gmail.com)

Abstract

The Greenland Ice Sheet (GrIS) responds rapidly to the present climate, therefore, its response to the predicted future warming is of concern. To learn more about the impact of future climatic warming on the ice sheet, decoding its behavior during past periods of warmer than present climate is important. However, due to the scarcity of marine studies reconstructing ice sheet conditions on the Northeast Greenland shelf and adjacent fjords, the timing of the deglaciation over marine regions and its connection to forcing factors remain poorly constrained. This includes data collected in fjords that encompass the Holocene Thermal Maximum (HTM), a period in which the climate was warmer than it is at present. This paper aims to use new bathymetric data and the analysis of sediment gravity cores to enhance our understanding of ice dynamics of the GrIS in a fjord and inner shelf environment as well as give insight into the timing of deglaciation and provide a palaeoenvironmental reconstruction of southwestern Dove Bugt and Bessel Fjord since the Last Glacial Maximum (LGM). ~~The swath bathymetry data displayed in this study is the first time the bathymetry for Bessel Fjord has become available.~~ North-south oriented glacial lineations, and the absence of pronounced moraines in southwest Dove Bugt, an inner continental shelf embayment (trough), suggests the southwards and offshore flow of Storstrømmen, the southern branch of the Northeast Greenland Ice Stream (NEGIS)~~,~~ ~~Storstrømmen~~. Sedimentological data suggests that an ice body, theorized to be the NEGIS, may have retreated from the region slightly before ~11.4 cal. ka ~~cal~~ BP. The seabed morphology of Bessel Fjord, a fjord terminating in southern Dove Bugt, includes numerous basins, separated by thresholds. The position of basin thresholds, which include some recessional moraines, suggest that the GrIS had undergone multiple halts or readvances during deglaciation, likely during one of the cold events identified in the Greenland Summit temperature records~~ (Kobashi et al., 2017)~~. A minimum age of 7.1 ~~ka~~ cal. ka BP is proposed for the retreat of ice through the fjord to or west of its present-day position in the Bessel Fjord catchment area. This suggests that the GrIS retreated from the marine realm in early Holocene, around the onset of the HTM~~Holocene Thermal Maximum~~ in this region, a period when the mean July temperature ~~according to Bennike et al., (2008)~~ was at least 2-3 °C higher than at present, and remained at or west of this onshore position for the remainder of the Holocene. The transition from predominantly mud to muddy sand layers in a mid-fjord core at ~4 ~~ka~~ cal. ka BP may be the result of increased sediment input from nearby and growing ice caps. This shift may suggest that in the ~~l~~Late Holocene (Meghalayan), a period characterized by a temperature drop to modern values, ice caps in Bessel Fjord probably fluctuated with greater sensitivity to climatic conditions than the NE sector of the GrIS.

1. Introduction

Ice mass loss from the Greenland Ice Sheet (GrIS) has accelerated during the 21 century, making it the largest individual contributor to sea level rise (King et al., 2020). This introduction of a substantial quantity of fresh water may have ramifications for global ocean circulations as well as the climate (Rahmstorf et al., 2015). Approximately 12% of the ice from the GrIS is transported to the coast through the Northeast Greenland Ice Stream (NEGIS) (Khan et al., 2014; Joughin et al., 2001) and therefore has a substantial impact on the mass balance of the ice sheet and a potential to contribute to sea level rise. Currently, two of the three marine terminating outlet glaciers that are supplied by the NEGIS are in retreat (Mouginot et al., 2015), where the southernmost branch, Storstrømmen in Dove Bugt (Figs. 1a & 1b), is currently in a building phase following a 1978-1984 surge (Khan et al., 2014; Reeh et al., 1994). While there are numerous ~~modern~~ studies on the current state of the NEGIS during the past decades to century, there is a scarcity of data concerning the position and dynamics of the ice stream, and other local Northeast Greenland outlet glaciers, on a multi-century to millennia scale over marine regions. Considering that the global mean temperature is expected to continue to rise (Stocker et al., 2013), and that the Arctic will experience an amplification effect (Cohen et al., 2014), looking to the past, especially during warmer than present periods (i.e., the Holocene Thermal Maximum (HTM)), may provide an important insight into the future behavior of the ice sheet.

Marine studies have found evidence for past advancement and retreat of the GrIS and NEGIS along the continental shelf offshore Northeast Greenland (Evans et al., 2009; Winkelmann et al., 2010; Arndt et al., 2015, 2017; Laberg et al., 2017; Arndt, 2018; Olsen et al., 2020; Syring et al., 2020; Davies et al., 2022; Hansen et al., 2022; Jackson et al., 2022). Geomorphological findings in Store Koldewey Trough (~76°N), a major shelf trough northeast of the study area (Fig. 1b), suggests that the ice sheet may have reached the shelf break in this area during the LGM (Last Glacial Maximum) (Laberg et al., 2017; Olsen et al., 2020). However, ~~F~~further north (~79.4°N), findings by Rasmussen et al. (2022) indicate that some regions near the shelf break were ~~is interpreted as being~~ ice free during the LGM ~~(Rasmussen et al., 2022),~~ despite Arndt et al. (2017) positioning ~~an area where~~ the ice front at ~~had~~ its maximum LGM position at the outer shelf ~~according to Arndt et al. (2017)~~. A concise understanding of the timing and dynamics of the ice sheet over the NE Greenland shelf during the subsequent deglaciation of the marine realm remains to be established as very few dated cores have been recovered. Terrestrial dating (e.g., cosmogenic nuclide dates and lake studies) has provided further insight into when terrestrial regions had become deglaciated, and how the climate has changed in these areas (e.g., Björck and Persson, 1981; Björck et al., 1994; Wagner et al., 2008; Klug et al., 2009a; Schmidt et al., 2011; ~~Briner et al., 2016;~~ Skov et al., 2020; Larsen et al., 2020). However, only recently has terrestrial data been integrated with marine data to establish a detailed deglaciation chronology of the shelf, coastal and fjord regions (Davies et al., 2022; Larsen et al., 2022).

Swath bathymetry and gravity cores data from southwestern Dove Bugt (i.e., Store Bælt) and Bessel Fjord (Fig. 1), presented for the first time in this study, has been used to further refine our understanding of how the GrIS responded to changes in palaeoclimatic conditions from the LGM through the Holocene, including the HTM. Through this analysis we aim to reconstruct regional ice dynamics from both full-glacial conditions and during overall retreat and put our findings into the larger context of the dynamics of the Northeast Greenland Ice Sheet during these periods. Additionally, this study aims to refine our understanding about the timing of deglaciation over marine areas and compare findings to nearby terrestrial regions including the Store Koldewey ~~island~~ and Hochstetter Forland/Shannon Ø. Results will also contribute to our understanding of palaeoenvironmental conditions throughout the Holocene for the NE Greenland fjords and inner shelf areas.

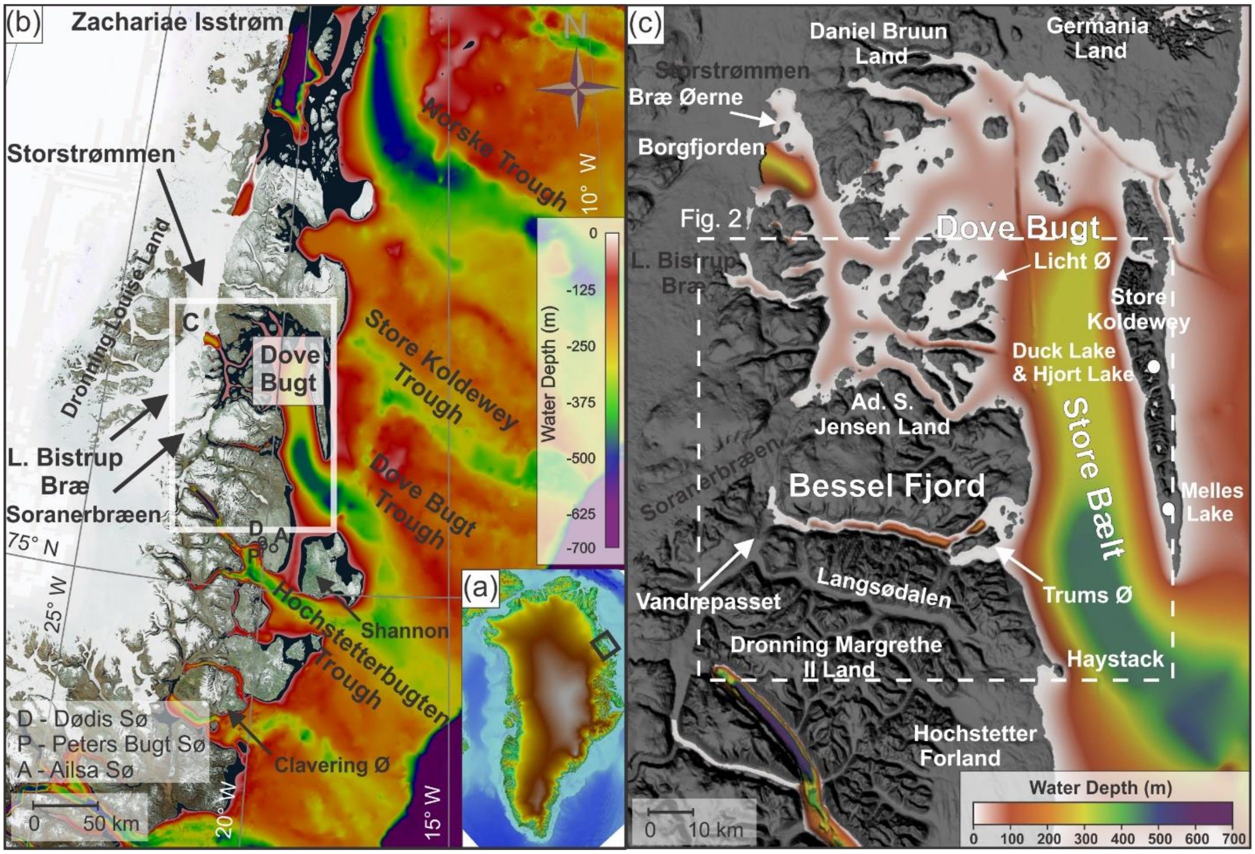

Figure 1. (a) An image of Greenland, using IBCAO 4.0 400x400m (Jakobsson et al., 2020)*, with a black box surrounding the study area. (b) Bathymetry of Northeast Greenland displayed using IBCAO 4.0 200x200m data* (Jakobsson et al., 2020) *and land is displayed using a World Imagery satellite image (Earthstar Geographics, Esri, HERE, Garmin, FAO, NOAA, USGS) made available through GlobalMapper. The white box surrounds the position of Fig. 1c. (c) Bathymetry of Dove Bugt and Bessel Fjord and surrounding land areas displayed using the IBCAO 4.0 200x200m data* (Jakobsson et al., 2020)*. Locations mentioned in the text are labelled here. The position of Fig. 2 is within the white dashed box.*

2. Regional Setting and Environmental History

Bessel Fjord is a west-east running fjord between Adolf S. Jensen Land and Dronning Margrethe II Land (Fig. 1c). The western end of the fjord contains the southern outlet glacier Soranerbræen, which also has a second outlet to the north in a tributary fjord to inner Dove Bugt (Fig. 2). Several ice caps are positioned across the length of the fjord (Figs. 2 & 3), some of which have several generations of moraines and glaciofluvial outlets that enter the fjord. Colluvial fans and rivers have been observed across the length of the fjord in satellite images and while surveying the fjord. Multiple islands are located at the entrance of Bessel Fjord, the largest of which, Trums Ø, splits the entrance into two main inlets (Figs. 1c & 2). From the termination of Soranerbræen to the entrance of the fjord measures ~60 km in length. The width of the fjord ranges from 1.8 to 3.7 km.

To the west of Bessel Fjord and Soranerbræen is the larger glacier L. Bistrup Bræ, which flows northwards and has an outlet in Borgfjorden, another tributary fjord to inner Dove Bugt (Fig 1). Here it is confluent with the southward flowing NEGIS outlet glacier, Storstrømmen (Rignot et al., 2022). Studies of modern Soranerbræen, L. Bistrup Bræ and Storstrømmen suggest that they all have separate drainage basins (Krieger et al., 2020). Storstrømmen and L. Bistrup Bræ are two of the largest surge-type glaciers in the world (Higgins, 1991) with a surge periodicity of approximately 70 years (Mouginot et al., 2018).

Bathymetry of inner Dove Bugt and tributary fjords has revealed that there are no natural large passageways for the warm, salty, subsurface Atlantic Intermediate Water to impact these glaciers at present, therefore it has been suggested that ocean waters do not play a large role in the evolution of Storstrømmen, L. Bistrup Bræ and the northern outlet of Soranerbræen, and that their grounding line retreat is mostly caused by ice thinning (Rignot et al., 2022).

Mega-scale glacial lineations (MSGL) identified in Store Koldewey Trough on the continental shelf have been interpreted as evidence for the expanse of this sector of the GrIS to the shelf break during the LGM (Laberg et al., 2017; Olsen et al., 2020). This is further supported by the presence of recessional moraines and grounding zone wedges, which suggests a complex deglaciation of this part of the shelf area (Arndt et al., 2015, 2017; Laberg et al., 2017; Arndt, 2018; Olsen et al., 2020). Olsen et al. (2020) has suggested that deglaciation in the Store Koldewey Trough may have occurred in two stages: first, an initial retreat as a result of eustatic sea level rise caused by melting ice at lower latitudes (Lambeck et al., 2014), followed by a melting phase driven by ocean warming. So far, the timing of the onset of the deglaciation is not known. Across the GrIS, deglaciation is believed to be asynchronous, with factors such as topography and local ice dynamics playing a large role with ice retreat in conjunction with climate change (Bennike & Björck, 2002; Funder et al., 2011; Ó Cofaigh et al., 2013; Hogan et al., 2016).

A recent study by Jackson et al. (2022) of the inner shelf east of the Clavering Ø (~74^{o} N; Fig. 1b) indicated that during the late Younger Dryas, this sector of the GrIS had reached a more landward position, in conformity with Funder et al. (2021). During this period, the inner shelf bottom water was characterized by anomalously high temperatures, interpreted to have played a role in the ice retreat and leading to the termination of the Younger Dryas stadial. This was followed by the onset of the East Greenland Current, as seen from cooler bottom water from the Early Holocene on (Jackson et al., 2022).

Further north, east of marine terminating glacier Zachariae Isstrøm (~78^{o} 30N; Fig. 1b), the deglaciation of the NEGIS from the inner shelf was found to have occurred as early as 12.5 ~~ka~~ cal. ka BP, likely before 13.4 ~~ka~~ cal. ka BP (Davies et al., 2022). Here, inflow of warmer water (Atlantic Water) may have played a role. This part of the shelf was covered by an ice shelf from 13.4 to 11.2 ~~ka~~ cal. ka BP (including the Younger Dryas), retreating and leading to open water conditions from the earliest Holocene; 11.2-10.8 ~~ka~~ cal. ka BP, before readvancing from 10.8 to 9.6 ~~ka~~ cal. ka BP, finally retreating from 9.6 to 7.9 ~~ka~~ cal. ka BP. At 7.9 ~~ka~~ cal. ka BP there was a drastic shift in ocean circulation at this site with a sharp decline in Atlantic Water corresponding to an increase in Polar Water influx (Davies et al., 2022). Pados-Dibattista et al. (2022), studying another core from the NE Greenland shelf (more seaward, in a mid-shelf position north of the Norske Trough at ~79^{o}N), found that during the early Holocene (9.4 to 8.2 ~~ka~~ cal. ka BP), the East Greenland Current was highly stratified with cold surface water overlying warm Atlantic subsurface water.

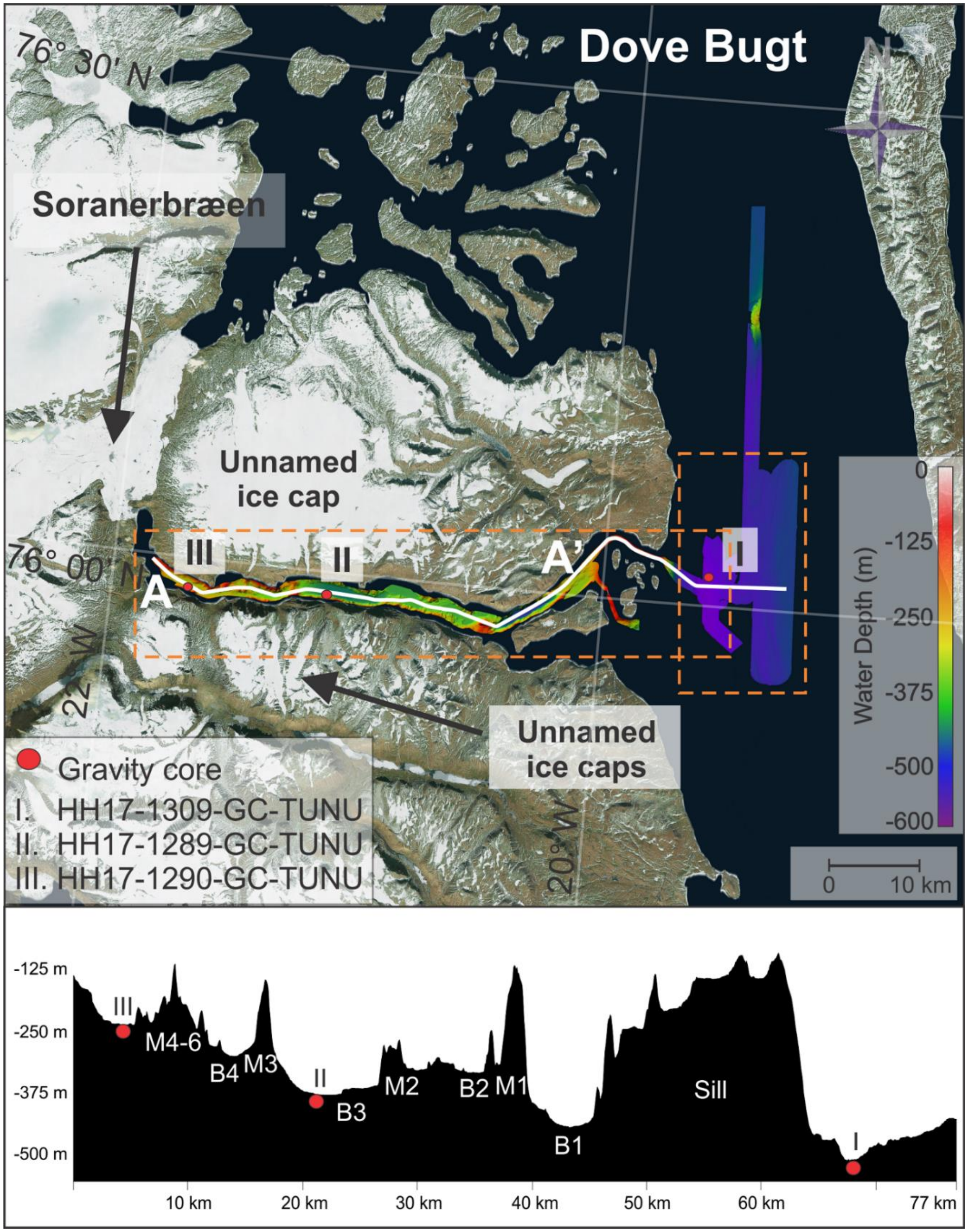

Figure 2. Study area with the bathymetric data showing the locations of the sediment cores presented in this study. The lower panel is a profile along the length of Bessel Fjord, A-A'. Sediment cores are labelled I, II and III. Satellite image is displayed using a World Imagery satellite image (Earthstar Geographics, Esri, HERE, Garmin, FAO, NOAA, USGS) made available through GlobalMapper.

Figure 3. Image of an ice lobe from an ice cap near gravity core HH17-1289-GC-TUNU. Two sets of coarse-grained terminal morainal ridges are indicated by numbers and arrow. See Fig. 6b for the position of the modern ice lobe. The photograph was taken by Torger Grytå on a 2017 TUNU cruise.

Following the 8.2 ka event, the interval from 8.2 to 6.2 ~~ka~~ cal. ka BP was followed by the warmest Holocene bottom water conditions on the shelf. Afterwards, conditions returned to those seen prior to 8.2 ~~ka~~ cal. ka BP due to increased Polar Water transport strengthening the East Greenland Current (Pados-Dibattista et al., 2022).

Terrestrial studies of Dronnings Margrethe II Land, Germania Land and adjacent areas have identified a complex assortment of moraines that are believed to have formed during the Kap Mackenzie, Muschelbjerg, Nanok I and Nanok II stadials (Hjort, 1979, 1981; Hjort and Björck, 1983; Björck et al., 1994; Landvik, 1994). The exact ages of these stadials remain unclear (Table 1), yet Larsen et al. (2022) suggests that Nanok-stadial moraines found in Store Koldewey formed synchronously with the Milne Land moraines of Scoresby Sund which date to the Allerød to early Younger Dryas and Preboreal time (Kelly et al., 2008; Levy et al., 2016).

The position of striations on Store Koldewey and lateral moraines on coastal slopes between Bessel Fjord and Haystack have been interpreted as evidence for ice flowing out of Dove Bugt and Bessel Fjord during the Muschelbjerg stadial, southwards through Store Bælt and turning eastwards around the southernmost mountains of Store Koldewey (Hjort, 1981). Early studies of the region noted glacial and glaciofluvial deposits (e.g., moraine plateau~~x~~, terminal moraines, eskers and sandurs) on Hochstetter Forland that are believed to have formed during this period (Hjort, 1979, 1981).

Table 1. Previously published stadial information for the Dove Bugt region as well as age estimates used in this study.

Stadials	**Studies**					**Age estimate used in this study**
	Hjort & Björck (1983)	*Funder et al., (1998)*	*Kelly et al. (2008)*	*Vasskog et al. (2015)*	*Larsen et al. (2022)*	
Nanok II	10.1-9.5 ka cal BP	Preboreal (ending at ca. 9.7 ka cal BP)	Younger Dryas and Early Holocene (13-11.6 ka cal BP (G-III), 11.7-10.6 ka cal BP (G II))	Close to Bølling– Allerød transition, and late Younger Dryas (~14 ka cal BP (G III), ~12 ka cal BP (G-II))	Preboreal	Preboreal
Nanok I	Older than 14 ka cal BP, possibly between 15 and 19 ka cal BP				Late Allerød to early Younger Dryas	Late Allerød to early Younger Dryas
Nanok 0		~48 ka (Hjort, unpublished data)				?
Muschelbjerg	Saalian (or older)?					Saalian (or older)?
Kap Mackenzie	Saalian (or older)?					Saalian (or older)?

Stadials	Studies					Age estimate used in this study
	Hjort & Björck (1983)	*Funder et al., (1998)*	*Kelly et al. (2008)*	*Vasskog et al. (2015)*	*Larsen et al. (2022)*	
Nanok II	10.1-9.5 cal. ka BP	Preboreal (ending at ca. 9.7 cal. ka BP)	Younger Dryas and Early Holocene (13-11.6 ka (G-III), 11.7-10.6 ka (G II))	Close to Bølling– Allerød transition, and late Younger Dryas (~14 cal. ka BP (G III), ~12 cal. ka BP (G-II))	Preboreal	Preboreal
Nanok I	Older than 14 cal. ka BP, possibly between 15 and 19 cal. ka BP				Late Allerød to early Younger Dryas	Late Allerød to early Younger Dryas
Nanok 0		~48 cal. ka BP (Hjort, unpublished data)				?
Muschelbjerg	Saalian (or older)?					Saalian (or older)?
Kap Mackenzie	Saalian (or older)?					Saalian (or older)?

Lateral moraines and glacial striations oriented along the axis of Langsodal (also referred to as Langsødalen; Fig. 1c), a nearby valley south of and sub-parallel to Bessel Fjord, have been interpreted as evidence for glacial confinement within the valley during an undifferentiated Nanok stadial (Hjort 1979; Hjort, 1981). This differs from striations that have also been identified in the valley along more weathered surfaces that are oriented in a southwestern direction (Hjort, 1979).

The outer coastal regions of North and Northeast Greenland are believed to have been deglaciated between 12.8 and 9.7 ka ~~cal~~ BP and present ice positions were reached between 10.8 to 5.8 ka ~~cal~~ BP (Larsen et al., 2022). Cosmogenic nuclide dates from Store Koldewey, first collected by Håkansson et al. (2007), and later Skov et al. (2020) and Larsen et al. (2022), suggest that ice retreated from the continental shelf and reached the upper and lower sections of the island by 12.3 and 12.7 ka ~~cal~~ BP, respectively. In contrast, Biette et al. (2020) found evidence of the deglaciation of Clavering Ø at 16.2 ka ~~cal~~ BP, with readvances at 11.3, 10.8, 3.3, 1.2 and 0.37 ka ~~cal~~ BP. Additional cosmogenic nuclide findings indicate that Trums Ø, in outer Bessel Fjord, may have become deglaciated around 12.6 ka ~~cal~~ BP and Vandrepasset, onshore inner Bessel Fjord~~,~~ by 8.6 ka ~~cal~~ BP (Larsen et al., 2022).

Findings from macrofossil remains (Bennike & Björck, 2002) and lacustrine sedimentary records (Cremer et al., 2008) suggest that coastal regions were deglaciated in a ~1500 year span after the start of the Holocene (Klug et al., 2016). To the north of Store Koldewey, a minimum date for deglaciation in Germania Land of 9.5 ~~ka~~ cal. ka BP has been proposed (Landvik, 1994), whereas to the south in southern Dronning Margrethe II Land, a minimum date of 11.2 ~~ka~~ cal. ka BP has been suggested (Bennike & Weidick, 2001). Lake studies on aquatic organisms at Björck Lake and Hjort Lake on Store Koldewey (Fig. 1c) indicate that the island was at its warmest between ~8 and 4 ~~ka~~ cal. ka BP, (Wagner et al., 2008; Klug et al., 2009; Schmidt et al., 2011), although findings from Melles Lake (Fig. 1c) suggest that the earliest onset of warmth during the Holocene may have occurred at ~ 10 ~~ka~~ cal. ka BP (Klug et al., 2009; Briner et al., 2016). On Hochstetter Forland (Fig. 1c), pollen assemblages from Dødis Sø, Peters Bugt Sø and Ailsa Sø suggest that the temperatures were at their highest between 8.8 and 5.6 ~~ka~~ cal. ka BP (Björck & Persson, 1981; Björck et al., 1994). These findings indicate that the HTM was not uniform across East Greenland, as also described by Briner et al. (2016).

To the south, offshore the Kejser Franz Josef ~~f~~Fjord system (~73°N), a detailed biomarker record finds this part of the shelf dominated by seasonal sea ice throughout the ~~l~~Late Holocene (<~5 ~~ka~~ cal. ka BP) and extended concentrations from 5.2 to 2.2 and 1.3 cal. ka BP to present. Short-term variability was also seen for this area for the last 2.2 ~~ka~~ cal. ka BP, corresponding to the climatic events of this period (Kolling et al., 2017).

3. Material and Methods

Swath bathymetry and three sediment cores were collected in southwestern Dove Bugt and Bessel Fjord during an expedition aboard RV *Helmer Hanssen* of UiT The Arctic University of Norway in September 2017, being part of the TUNU program (Fig. 2; Christiansen, 2012). The swath bathymetry data was obtained using a Kongsberg Maritime Simrad EM 302 multibeam echo sounder. It was gridded using Petrel software, and geomorphological interpretations were made using Global Mapper 18. Surfaces were developed using a 5x5m grid cell size while a surface created from an International Bathymetric Chart of the Arctic Ocean (IBCAO) dataset 4.0 with a 200x200m grid cell size (Jakobsson et al., 2020).

Two soft sediment gravity cores were retrieved from Bessel Fjord (HH17-1289-GC-TUNU & HH17-1290-GC-TUNU) and one southwest of Dove Bugt in the sound Store Bælt (HH17-1309-GC-TUNU) (Fig. 2 & Table 2). Prior to splitting the cores, physical properties were measured using a GEOTEK Multi Sensor Core Logger (MSCL-S). The cores were placed in the laboratory for 24 hours prior to obtaining physical measurements to ensure that each core temperature reached equilibrium with the laboratory to avoid distorting p-wave values (Weber et al., 1997).

A GEOTEK MSCL X-ray Computed Tomographic imaging machine was also used to scan the unopened core sections to create X-ray radiographic images. After each core was split and cleaned, the characteristics of the sedimentary surface were logged (i.e., structures, bioturbation, grain size, lithological boundaries, etc.), sediment color was noted using the Munsell Soil Color Chart and lithofacies were assigned based on Eyles et al. (1983) classification system. ~~X-ray fluorescence (XRF) data (not published here), as well as c~~Colored images of the core sections~~,~~ were then obtained using an Avaatech XRF core scanner.

Table 2. Information on the position, water depth and recovery length of each gravity core. Note that the core names are abbreviated in the text.

Location	**Inner Bessel Fjord**	**Mid-Bessel Fjord**	**Southeastern Dove Bugt**
Coring station	HH17-1290	HH17-1289	HH17-1309
Latitude [N]	75° 58' 34.5907"	75° 58' 11.4928"	76° 01' 34.0387"
Longitude [W]	21° 07' 13.1055"	21° 41' 48.0278"	19° 34' 31.3190"
Water depth [m]	372	225	512
Recovery [cm]	534.5	245.5	474.55

Molluscs and benthic foraminifera were recovered from each core for the purpose of radiocarbon dating of lithofacies boundaries. This was, however, not always possible due to the low content of foraminifera and molluscs in these cores which also restricted the number of dates that could be obtained. Two adjacent 1 cm thick sediment slices were successfully sampled from select positions across cores HH17-1290 and HH17-1309. Samples were then wet sieved at 1 mm, 100 µm and 63 µm meshes, respectively. Benthic foraminifera from the 100-um size fraction were extracted for radiocarbon dating. Radiocarbon dating was carried out at the MICADAS radiocarbon laboratory at Alfred Wegener Institute, Helmholtz Centre for Polar and Marine Research, Germany. The radiocarbon dates were calibrated using the online version of OxCal 4.4 (https://c14.arch.ox.ac.uk/oxcal.html#program) and the Marine20 calibration curve (Heaton et al., 2020), as the calibrated ^{14}C samples are younger than 11.5~~ ka~~ cal. ka BP (Heaton et al., 2022). We are using a ΔR of -10 ± 60 in conformity with Jackson et al. (2022). Previously reported radiocarbon dates from this area that are relevant to our study have been recalibrated using Marine20 for marine samples under 11.5 cal. ka BP and IntCal20 for terrestrial samples (Reimer et al., 2020). One marine sample older than 11.5 ~~ka~~ cal. ka BP has also been included (Table 3). ~~We are aware that for~~ In the Arctic, including our study area, calibration of marine samples by Marine20 is not recommended for samples older than 11.5 cal. ka BP (see Heaton et al. (2022)), therefore, this calibrated age is treated with caution.

A Beckman Coulter LS 13 320 Multi-Wavelength Laser Diffraction Particle Size Analyzer was used to perform sediment grain size analysis. Sediment was sampled in mostly 10 cm intervals across HH17-1309, where samples taken from the other two cores were selected from specific positions. Samples were treated in HCl and H_2O_2 and a pre-heated VWB 18 Thermal Bath. Samples were then cleaned using distilled water, placed through multiple runs through a centrifuge and heated in an oven to remove water content. Approximately 0.2 grams of sediment were then separated and placed in a container with 20 ml of water and moved to a shaking table for over 48 hours. A few drops of Calgon were added to each sample, which was then placed into a Branson 200 ultrasonic cleaner for ~7 minutes and shaken briefly before being poured through a >2 mm mesh and into the particle size analyzer. Grains between the size of 0.4 µm and 2000 µm were counted and underwent three separate runs. GRADISTAT Excel-software was used to calculate the mean of the three runs. Sediment names used in reference to this analysis are based on Folk (1954) and mean grain size from the methodology published by Folk & Ward (1957).

*Table 3. Other published radiocarbon dates and their recalibrated ages using Marine20 (and an ΔR of -10 ± 60 in conformity with Jackson et al. (2022)) and IntCal20 for aquatic moss samples. *The age of sample Lu-1298 from Shannon is above what is recommended by Heaton et al., (2022) for use with Marine20. ~~and is therefore treated with~~*

~~caution~~. This date was considered an outlier and therefore not taken into consideration by the authors and Bennike and Björck (2002). Therefore, this date is also rejected in the present study.

Location	Material	Lab nr.	^{14}C age	^{14}C cal BP (1 σ range)	^{14}C cal BP (median)	Reference
Shannon	shell	Lu-1298*	19000 ± 190	21855-22325	22078	Hjort, 1981; Hjort 1979
Hochstetter F.	shell	Lu-1289	9190 ± 90	9572-9926	9779	Hjort, 1981; Hjort 1979
Shannon	shell	Lu-1389	9370 ± 90	9865-10195	10015	Hjort, 1981; Hjort 1979
Hochstetter F.	shell	Lu-1386	9400 ± 90	9896-10220	10054	Hjort, 1981; Hjort 1979
Hochstetter F.	shell	Lu-1300:1	9470 ± 90	9970-10322	10157	Hjort, 1981; Hjort 1979
Hochstetter F.	shell	Lu-1300:2	9520 ± 90	10084-10412	10229	Hjort, 1981; Hjort 1979
Hochstetter F.	shell	Lu-1384	9810 ± 95	10409-10794	10617	Hjort, 1981; Hjort 1979
Ardencaple Fjord	shell	Lu-1390	8570 ± 85	8864-9200	9022	Hjort, 1981; Hjort 1979
Kildedalen	shell	Lu-1303	8930 ± 90	9290-9573	9447	Hjort, 1981; Hjort 1979
Snenæs	Mya truncata, Hiatella arctica	T-9372	8265 ± 95	8434-8768	8619	Landvik 1994
Hvalrosodden moraine	Nuculana pernula	TUa-123	8685 ± 95	9006-9315	9166	Landvik 1994
Hvalrosodden moraine	Nuculana pernula	TUa-124	9045 ± 90	9438-9741	9596	Landvik 1994
Hvalrosodden	Mya truncata	T-9361	8190 ± 95	8360-8663	8523	Landvik 1994
~~Hvalrosodden~~	Mya truncata, ~~Hiatella arctica~~	~~T-9370~~	~~7930 ± 120~~	~~8681-9085~~	~~8890~~	~~Landvik 1994~~
Hvalrosodden	Mya truncata	T-9371	7490 ± 115	8186-8502	8348	Landvik 1994
Peters Bugt	Portlandia arctica	Ua-2787	10260 ± 105	11071-11444	11253	Björck, 1994
Peters Bugt Sø	Hiatella arctica	Lu-3516	9640 ± 90	10222-10527	10382	Björck, 1994
Storstrømmen Sound	Mya truncata & Hiatella arctica	K-6098	5180 ± 95	5220-5520	5352	Weidick et al., 1994
Storstrømmen Sound	Mya truncata	K-5494	4910 ± 85	4865-5175	5028	Weidick et al., 1994
Storstrømmen Sound	Mya truncata	K-5493	4840 ± 90	4793-5117	4943	Weidick et al., 1994
Storstrømmen Sound	Hiatella arctica	Ua-3347	5030 ± 75	5023-5311	5166	Weidick et al., 1994
Storstrømmen Sound	Hiatella arctica	Ua-3350	4180 ± 60	3944-4225	4082	Weidick et al., 1994
Storstrømmen Sound	Balanoptera physalus	K-6096	3630 ± 90	3230-3530	3380	Weidick et al., 1994
Storstrømmen Sound	Hiatella arctica	Ua_3349	3725 ± 60	3371-3616	3496	Weidick et al., 1994
Storstrømmen Sound	Hiatella arctica & Mya truncata	K-6097	3230 ± 85	2749-3024	2897	Weidick et al., 1994
Storstrømmen Sound	Hiatella arctica	Ua-3348	1815 ± 55	1115-1317	1217	Weidick et al., 1994
Hjort Lake	Warnstorfia exannulata	Poz-6194	8260 ± 50	8456-8722	8602	Wagner, 2008
Duck Lake	Aquatic moss	LuS-6525	8690 ± 230	9527-10145	9775	Klug 2009

Location	Material	Lab nr.	^{14}C age	^{14}C cal BP (1 σ range)	^{14}C cal BP (median)	Reference
Shannon	shell	Lu-1298*	19000 ± 190	21855-22325	22078	Hjort, 1981; Hjort, 1979
Hochstetter F.	shell	Lu-1289	9190 ± 90	9572-9926	9779	Hjort, 1981; Hjort, 1979
Shannon	shell	Lu-1389	9370 ± 90	9865-10195	10015	Hjort, 1981; Hjort, 1979
Hochstetter F.	shell	Lu-1386	9400 ± 90	9896-10220	10054	Hjort, 1981; Hjort, 1979
Hochstetter F.	shell	Lu-1300:1	9470 ± 90	9970-10322	10157	Hjort, 1981; Hjort, 1979
Hochstetter F.	shell	Lu-1300:2	9520 ± 90	10084-10412	10229	Hjort, 1981; Hjort, 1979
Hochstetter F.	shell	Lu-1384	9810 ± 95	10409-10794	10617	Hjort, 1981; Hjort, 1979
Ardencaple Fjord	shell	Lu-1390	8570 ± 85	8864-9200	9022	Hjort, 1981; Hjort, 1979
Kildedalen	shell	Lu-1303	8930 ± 90	9290-9573	9447	Hjort, 1981; Hjort, 1979
Snenæs	Mya truncata, Hiatella arctica	T-9372	8265 ± 95	8434-8768	8619	Landvik, 1994
Hvalrosodden moraine	Nuculana pernula	TUa-123	8685 ± 95	9006-9315	9166	Landvik, 1994
Hvalrosodden moraine	Nuculana pernula	TUa-124	9045 ± 90	9438-9741	9596	Landvik, 1994
Hvalrosodden	Mya truncata	T-9361	8190 ± 95	8360-8663	8523	Landvik, 1994
Hvalrosodden	Mya truncata, Hiatella arctica	T-9370	7930 ± 120	8681-9085	8890	Landvik, 1994
Hvalrosodden	Mya truncata	T-9371	7490 ± 115	8186-8502	8348	Landvik, 1994
Peters Bugt	Portlandia arctica	Ua-2787	10260 ± 105	11071-11444	11253	Björck et al., 1994
Peters Bugt Sø	Hiatella arctica	Lu-3516	9640 ± 90	10222-10527	10382	Björck et al., 1994
Storstrømmen Sound	Mya truncata & Hiatella arctica	K-6098	5180 ± 95	5220-5520	5352	Weidick et al., 1994
Storstrømmen Sound	Mya truncata	K-5494	4910 ± 85	4865-5175	5028	Weidick et al., 1994
Storstrømmen Sound	Mya truncata	K-5493	4840 ± 90	4793-5117	4943	Weidick et al., 1994
Storstrømmen Sound	Hiatella arctica	Ua-3347	5030 ± 75	5023-5311	5166	Weidick et al., 1994
Storstrømmen Sound	Hiatella arctica	Ua-3350	4180 ± 60	3944-4225	4082	Weidick et al., 1994
Storstrømmen Sound	Balanoptera physalus	K-6096	3630 ± 90	3230-3530	3380	Weidick et al., 1994
Storstrømmen Sound	Hiatella arctica	Ua-3349	3725 ± 60	3371-3616	3496	Weidick et al., 1994
Storstrømmen Sound	Hiatella arctica & Mya truncata	K-6097	3230 ± 85	2749-3024	2897	Weidick et al., 1994
Storstrømmen Sound	Hiatella arctica	Ua-3348	1815 ± 55	1115-1317	1217	Weidick et al., 1994
Hjort Lake	Warnstorfia exannulata	Poz-6194	8260 ± 50	8456-8722	8602	Wagner et al., 2008
Duck Lake	Aquatic moss	LuS-6525	8690 ± 230	9527-10145	9775	Klug et al., 2009

4. Results

4.1. Seafloor landforms in SW Dove Bugt (Store Bælt)

4.1.1. Elongated Lineations - Glacial Lineations

Slightly curved sub-parallel lineations, oriented sub-parallel to the axis of Dove Bugt, are the most pronounced landforms in this part of the study area. They are oriented N-NW in the south and N-NE in the north (Fig. 4). The most frequently identified positive lineations (ridges) are 35-50 m in width, <1-3 m in height and between 1 and 10 km in length. Length to width ratios are frequently >10:1. At elevations shallower than 435 m depth, near the center of Store Bælt, the lineations are wider (e.g., 60-150 m wide), and occasional merging and overlapping of lineations occur (Fig. 4e). Wider lineations, often identified in the southern section of the study area (Fig. 4b), have also been identified with widths, lengths and heights ranging from 200-650 m, 3-8 km, and 4.5-15 m, respectively. Length to width ratios here are 7:1 to >10:1. Some of the larger lineations are superimposed by smaller lineations. Lateral ridges have also been identified in clusters overprinting the lineations (Fig. 4c), where furrows have been found cross cutting lineations (Fig. 4d). Lateral ridges measure 0.5 to 2 m in height and are approximately 45 to 250 m apart.

These elongated lineations are interpreted as glacial lineations (e.g., Ó Cofaigh, 2005). The thinner, more common lineations (with length/width-ratios >10:1) have been interpreted as mega-scale glacial lineations (MSGL), and such landforms are commonly associated with palaeo-ice stream environments (e.g., Stokes & Clark, 2001). Glacial lineations have been identified in numerous continental shelf regions around Greenland (Evans et al., 2009; Dowdeswell et al., 2014; Slabon et al., 2016; Laberg et al., 2017; Newton et al., 2017; Arndt, 2018; Batchelor et al., 2018; Jakobsson et al., 2018). While the mechanism behind the formation of these features are still being debated, some authors have suggested that they may have formed through meltwater flooding (Shaw et al., 2008), groove-ploughing (Clark et al., 2003) or the transverse flow in basal ice (Schoof and Clarke, 2008). King et al. (2009)~~, who viewed the formation of MSGL in real time in West Antarctica~~ favored aspects of the dilatant till instability model~~, but with till properties~~ that could explain ~~ribbed moraine formation and~~ the development of MSGLs ~~these landforms~~ on a decadal timescale. Sets of ridges that overprint the glacial lineations have been interpreted as recessional moraines, where furrows have been interpreted as iceberg plough marks.

4.1.2. Depression and Mound- Hill-Hole Pair

In northern Store Bælt, a 200 by 450 m wide, 3-4 m deep depression has been identified next to a mound with a width and height of 235 by 450 m and 3-4 m, respectively (Fig. 4d). The depression overprints N-S trending lineations, although the mound contains lineations on its surface.

This depression and mound have been interpreted as a hill-hole pair. These landforms can form when ice-thrust rafts of sediment are removed from the bed by cold-based, slow-flowing ice that transports the sediment that was once in the depression (Hogan et al., 2010; Klages et al., 2013, 2015). In this instance, a south bound ice stream may have removed frozen sedimentary material and deposited it further south. This interpretation is in conformity with studies from other high-latitude continental shelves where subglacial hill-hole pairs are interpreted as formed by ice frozen to the seafloor bed (Sættem, 1990; Ottesen et al., 2005).

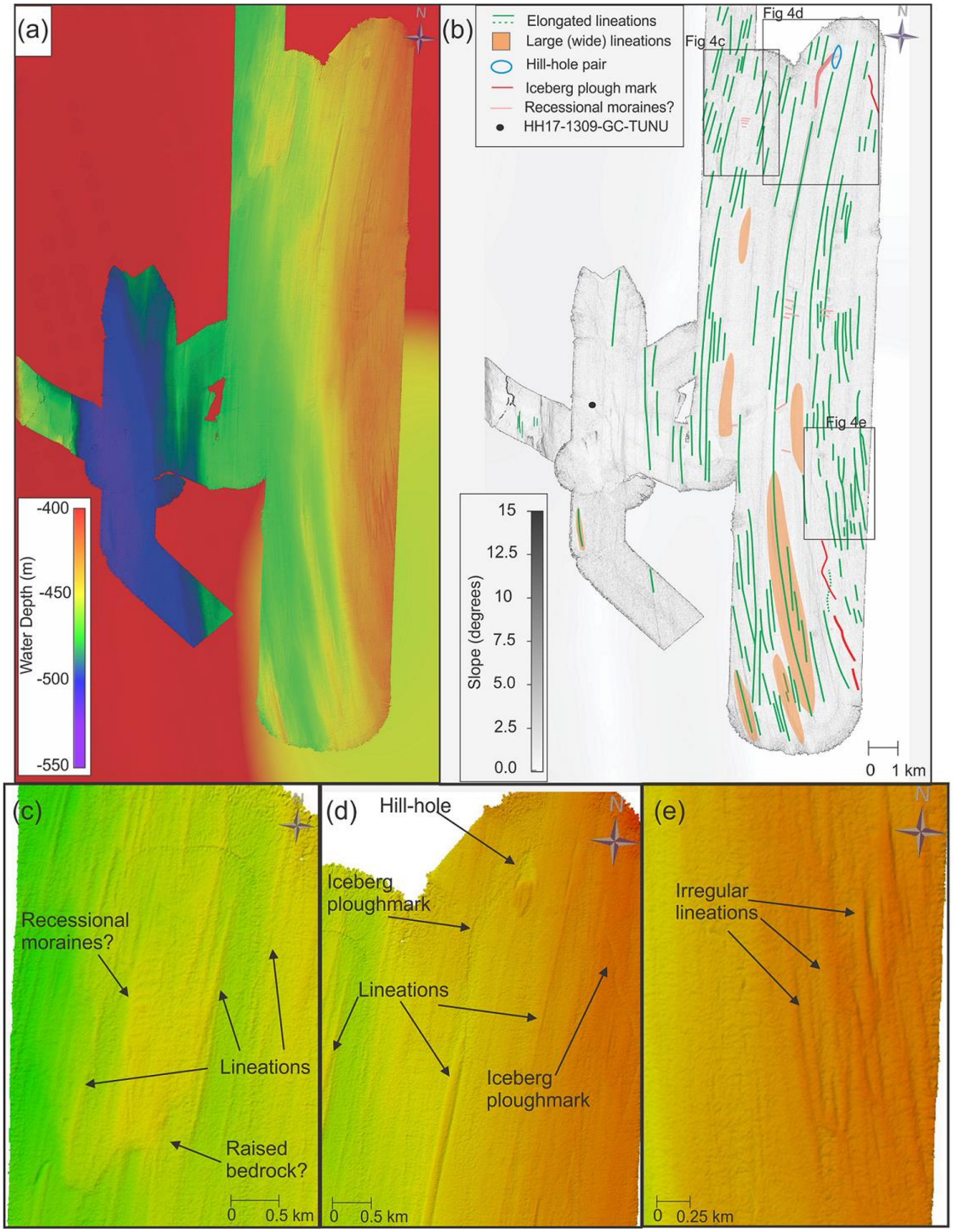

Figure 4. Bathymetric maps from SW Dove Bugt. (a) Seafloor relative to water depth with IBCAO 4.0 displayed in the background (Jakobsson et al., 2020)*. (b) The main landforms and slope angles of the seafloor in SW Dove Bugt. Locations of Figs. 4c-e are indicated. (c) Bathymetry of the northwestern section of the study area. (d) Bathymetry of the northeaster part of the study area. (e) Bathymetry of the eastern part of the study area showing irregularly shaped glacial lineations.*

4.2. Sea floor landforms in Bessel Fjord

4.2.1. Large scale geomorphology

Bessel Fjord contains a variety of basins that are separated by different styles of sills (Figs. 2, 5 & 6). The outermost sill is at the fjord's entrance, and it commonly ranges in depth from 50 to 200 m, with major sections reaching above (and near) the water surface as there are islands in the fjord entrance. Four large basins that are elongated in a west-east direction have been identified in Bessel Fjord (B1-B4). The deepest basin, Basin 1 (B1), is the closest to the fjord entrance and is separated from basin 2 (B2) by a >215 m high sill (M1) that is steeper to the east (Figs. 2 & 5). Basin 3 progressively deepens westwards, with a maximum depth of 380 m. A ~70 to 160 m asymmetrical sill (M3; Figs. 2 & 5) that is steeper on its east side separates Basin 3 from basin 4. Basin 4 is the shallowest basin (~280-300 m) and is adjacent to multiple smaller basins that are primarily at lower points of elevation. The fjord also contains smaller basins that are raised relative to the average seafloor depth (Fig. 6e). Features interpreted as bedrock mounds have also been identified in other sections of the fjord (Figs. 5 & 6). Along the fjord sides, landforms from sediment reworking including slide scars, channels and gullies have also been observed Fig 6b.

4.2.2. Linear Ridges Oriented Along Fjord Axis- Glacial Lineations

Oriented along the fjord's axis (or at times slightly oblique to it), linear features have been identified in the inner and middle of the fjord, as well as a single lineation on the outer part of the fjord (Figs. 5 & 6). They range in size from 100 to 1000 m in length and ~3 to 9 m in height, although some that are as high as 80 m have been identified in the inner fjord. Their morphologies vary throughout the fjord, and their length to width ratios range from 2:1 to 5:1. Most ridges slope towards the outer fjord, although some slope in the opposite direction or have an irregular or flat top. They appear both independently in connection with inferred bedrock highs, and in clusters in flat lying areas of basin 3. These ridges have been interpreted as glacial lineations, and they are thus indicating the direction of former glacier flow.

4.2.3. Transverse Ridges- Moraines

Several transverse ridges have been identified in the inner and central portion of the fjord, oriented perpendicular to the fjord's axis (Figs. 2, 5 & 6). The ridges in the inner most position of the fjord tend to largely conform to the topography (i.e., between bedrock mounds, some of which are position mid-fjord (M4-6; Fig. 6b), and the fjord sidewalls) and are the threshold between sub-basins (Fig. 6). The width and length of ridges range from 150 to 600 m and 120 to 500 m, respectively, where their heights are between <5 to 58 m.

A particularly large, asymmetrical transverse ridge that spans the width of the fjord, is situated between Basin 3 and 4 (M3; Figs. 2 & 6d). This ridge is ~1.5 km in width and between 72 to 162 m in height. It contains a crescent shape in aerial view and is concave towards the mouth of the fjord. A large threshold with a 1.8 km width and a > 215 m height also separates basin 1 and 2 (M1; Figs. 2 & 5). This feature is ~150m shallower in the north and dips steeply into basin 1.

The transverse ridges have been interpreted as moraines, which would have formed during glacial stillstands or readvancements during the retreat of a grounded tidewater glaciers margin. These moraines do not fill the width of the innermost fjord, which has also been seen in inner Nordfjord (part of the Keiser Franz Josef fjord system) by Olsen et al. (2022). While the large transverse ridge M3 is believed to be a moraine, it is considered more likely that M1 is a bedrock mound based on its morphology. The smaller transverse ridges are interpreted as recessional moraines. Smaller moraines have the potential to form at ice margins annually

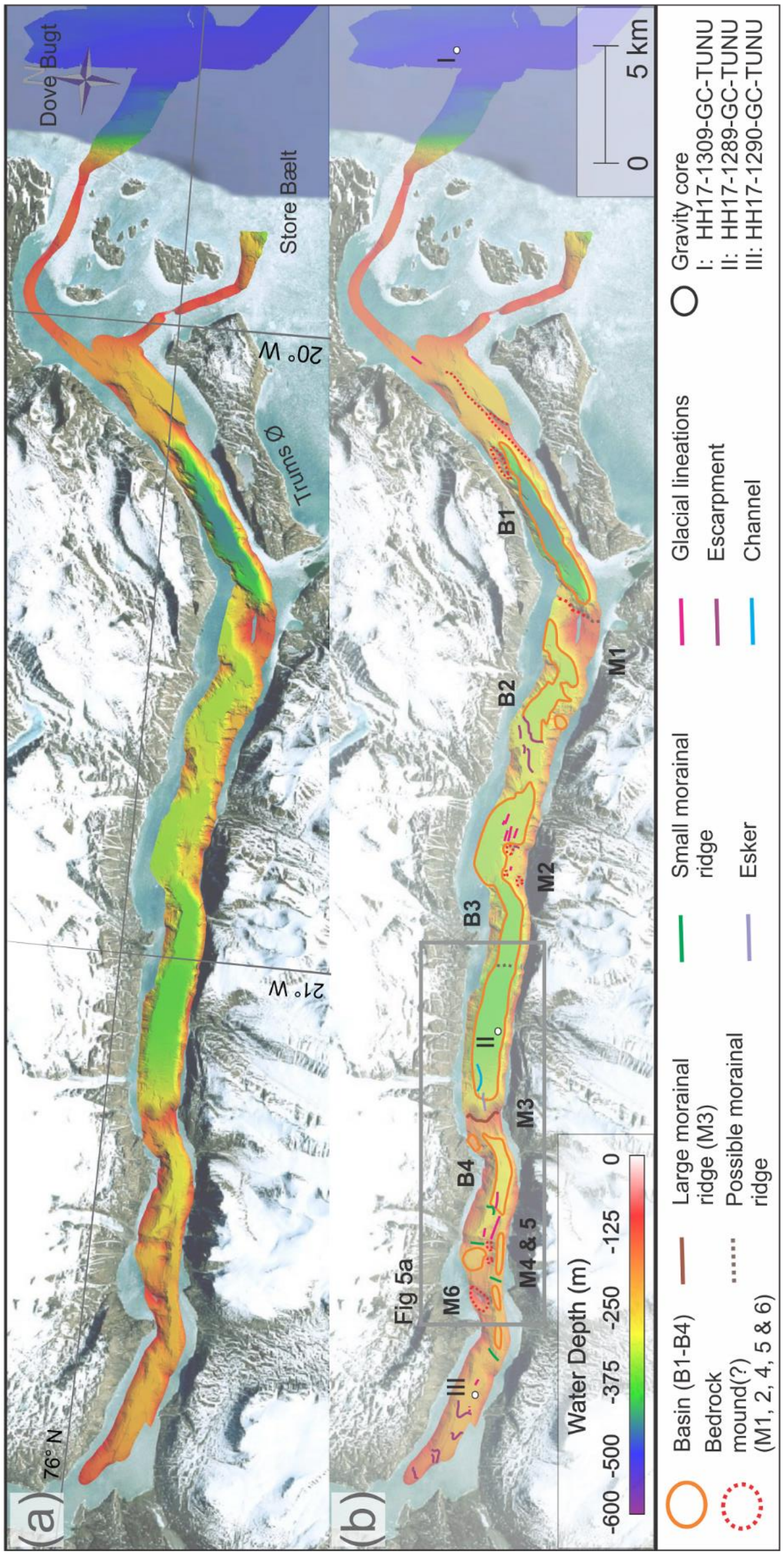

Figure 5. (a) Bathymetric map of Bessel Fjord. (b) A map of mapped features in Bessel Fjord. Satellite images obtained from Google Earth (© Google 2020).

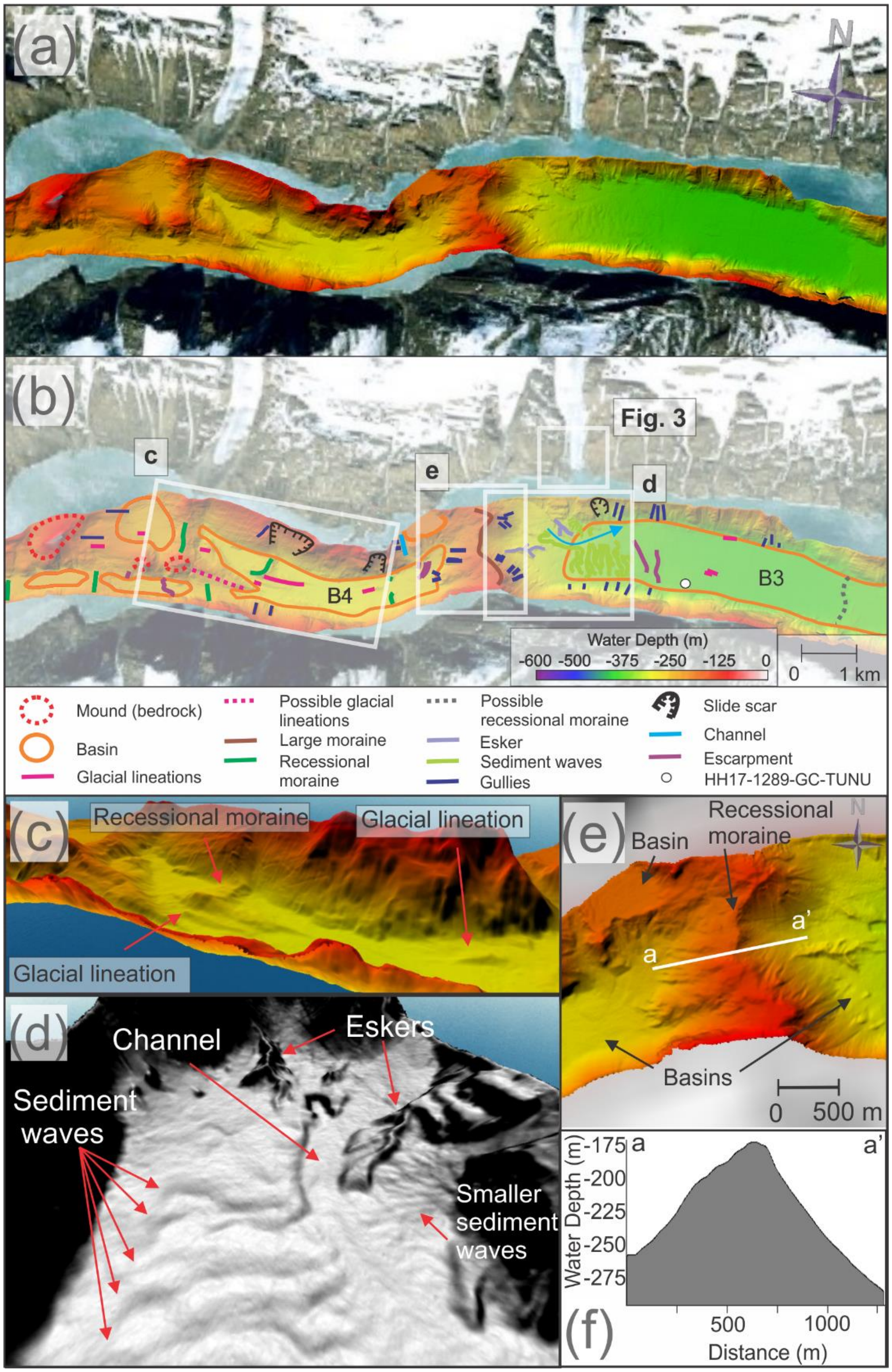

Figure 6. (a-b) Mapped sections from inner to middle Bessel Fjord. Background images used for 6a & 6b obtained from Google Earth (© Google 2020). (c) Glacial lineations in Basin 4 (B4). (d) Eskers, sediment waves and a channel in Basin 3 (B3). (e) A large moraine (M3) between B3 and B4. Note the raised sub-basin to the west and esker to the east. (f) Profile across the large recession moraine (M3).

(Lyså & Vorren, 1997; Dowdeswell et al., 2016) and have been observed with a variety of sizes and morphologies on the NE Greenland shelf (e.g., Winkelmann et al., 2010).

4.2.4. Sinuous Ridges- Eskers

Sinuous ridges, oriented parallel or oblique to the fjord's axis, occur in basin 3 (Figs. 5, 6b, 6d &6e). These features have widths and lengths of 50 to 120 m, 350 to 800 m, respectively and heights of 10 to 15 m. The most pronounced examples of these ridges have been observed east of the large recessional moraine that has been previously discussed (Fig. 6e).

These sinuous ridges have been interpreted as eskers. These landforms form from sediment infill of subglacial and englacial conduits and have been identified in other studies in Greenland (Huddart and Lister, 1981; Geirsdóttir et al., 2000; Winkelmann et al., 2010; Lane et al., 2015). They frequently form in the direction of former ice flow and often form during terminal stages of glaciation, and are therefore associated with moraines (Shreve, 1985). They vary in size depending on the glacial drainage pattern, as well as a number of other factors, however eskers identified within Bessel Fjord appear smaller than those identified in studies in Canada, the UK and Kola Peninsula in Russia (Storrar et al., 2014).

4.2.5. Wavy Transverse Ridges- Sediment Waves

Adjacent to the two eskers in Basin 3 are a series of wavy transverse ridges to the east of a large recessional moraine (Figs. 5, 6b & 6d). These features occupy an area of ~500 by 1500 m and contain small ridges and flat areas that slope at an angle of 3 to 6° to the east. Each wave "crest" is ~50 to 100 m apart, although some appear to begin only halfway through the width of the area, where others occupy the entire width, north to south. These waves are crosscut by a channel to the north (Fig. 6d). North of this channel similar features with a wavy morphology occur, although these are substantially smaller.

These wavy transverse ridges have been interpreted as sediment waves. Sediment waves found associated with deltaic and glacifluvial deltaic systems have been associated with retrogressive slope failures, gravity-induced sediment creep and/or the migration of sediment waves upslope (Cartigny et al., 2011; Hill, 2012; Stacey and Hill, 2016). Alternatively, given the position of the smaller wavy transverse ridges to the ice cap on Ad. S. Jensen Land (Figs. 1 & 2) and the larger ridges to the large moraine to the west (Figs. 5 & 6) it is also possible that these ridges are sets of moraines. Recessional moraines have been identified in the vicinity of eskers in Spitsbergen fjords (Ottesen et al., 2008; Kempf et al., 2013), which may account for the smaller wavy transverse ridges. The larger wavy transverse ridge do also resemble thrust moraines identified by Forwick et al. (2010). Further work may be required in the evaluation of these features. For a full list of observed landforms see Table 4.

4.3. Lithostratigraphy

Three gravity cores were retrieved from the study area. Gravity core HH17-1309 was collected in Store Bælt and was sampled from a N/NW-S/SE oriented depression that contains iceberg ploughmarks and a MSGL. Gravity core HH17-1289 was collected in the middle of the Bessel Fjord and is located directly east of the above-mentioned sediment waves on the distal part of the pronounced transverse ridge. Nearby, a modern ice cap fed glacifluvial channel is observed in satellite imagery, likely with a delta at its fjord termination. The gravity core HH17-1290 was collected within the inner fjord, west of the basins and thresholds observed in this study area and is the closest core to Soranerbræen (located ~9.7 km east of the glacier) (Fig. 7).

Table 4. Overview of observed landforms in southern Dove Bugt and Bessel Fjord.

Region	Description	Width	Length	Height	Notable Feature	Interpretation
Dove Bugt	Elongated lineations	35-50 m	~1->10 km	<1-3 m	Roughly N-S	Glacial Lineations
	**Wide*	200-650 m	3.8 to 8.8. km	4.5-15 m		
	Depression and mound	200 m	450 m	3-4 m	Mound to the south of the depression	Hill-hole pair
	Furrows (scour marks)	~40-100 m	<100-200	3-5 m	Irregular	Iceberg plough marks
	Transverse ridges	150-400 m	~30-100 m	0.5-1 m	Roughly W-E	Recessional moraines
Bessel Fjord	Linear ridge	45-350 m	100-1000 m	3-9, 80 m	Parallel to the fjords axis	Glacial Lineations
	Transverse ridges	150-600 m	120- 500 m	<5-58 m	Perpendicular to the fjords axis	Recessional moraines
	**Large ridge (M3)*	1485 m	600-1600 m	72 to 162 m		Moraine
	Sinuous ridges	50-120 m	350-800 m	10-15 m		Esker
	Wavy transverse ridges	400-700 m	~45-100 m	2-5 m	Perpendicular to the fjords axis	Sediment wave
	Elongated depression	~200 m	~1 km	6-8 m		Channels
	Chute	~20-100 m	60-400 m	1-15 m		Gullies

4.3.1. Facies

Facies 1 – Laminated Mud (Fl, Fl-d & Fl/m-d)

Facies 1 consists of laminated mud (Fl) and laminated mud with dropstones (Fl-d) and have been observed in all three gravity cores (Figs. 7, 8a, 8d & 8f)~~)~~. Laminations are composed of either mud or very fine sand. Mud laminations with finer laminations have also been identified in Unit 3.2 (100-200 cm; Fig. 7a, Fl/m-d). Microfractures have also been identified within this facies (Fig. 8f).

Wet-bulk density measurements tend to increase with depth in some sections of this facies (e.g., 87-350 cm in HH17-1309), suggesting normal sediment consolidation. However, a stagnation or decrease in wet-bulk density with depth in other sections (e.g., below ~350 cm in HH17-1309) suggests less consolidation. The magnetic susceptibility generally tends to increase with depth in HH17-1309 and in Unit 3.2 in HH17-1290, however the remainder of this facies in HH17-1290 (Unit 3.1) remains relatively stable to the base of the core. Notable positive peaks have been identified at 110 and 140 cm in HH17-1309 and measurement fluctuations occur in HH17-1289. Peaks in magnetic susceptibility may reflect the introduction of turbidites or clasts where fluctuations may reflect shifts in sediment provenance.

Muds with sand laminations are believed to have formed through a combination of ice-proximal suspension settling from overflow plumes and turbidity-current activity (underflows). The rhythmically laminated muds are believed to have formed from ice-proximal suspension settling from turbid overflow plumes. Similar laminated sediments have been identified in Kejser Franz Joseph Fjord and Fosters Bugt in East Greenland and are theorized to have been deposited

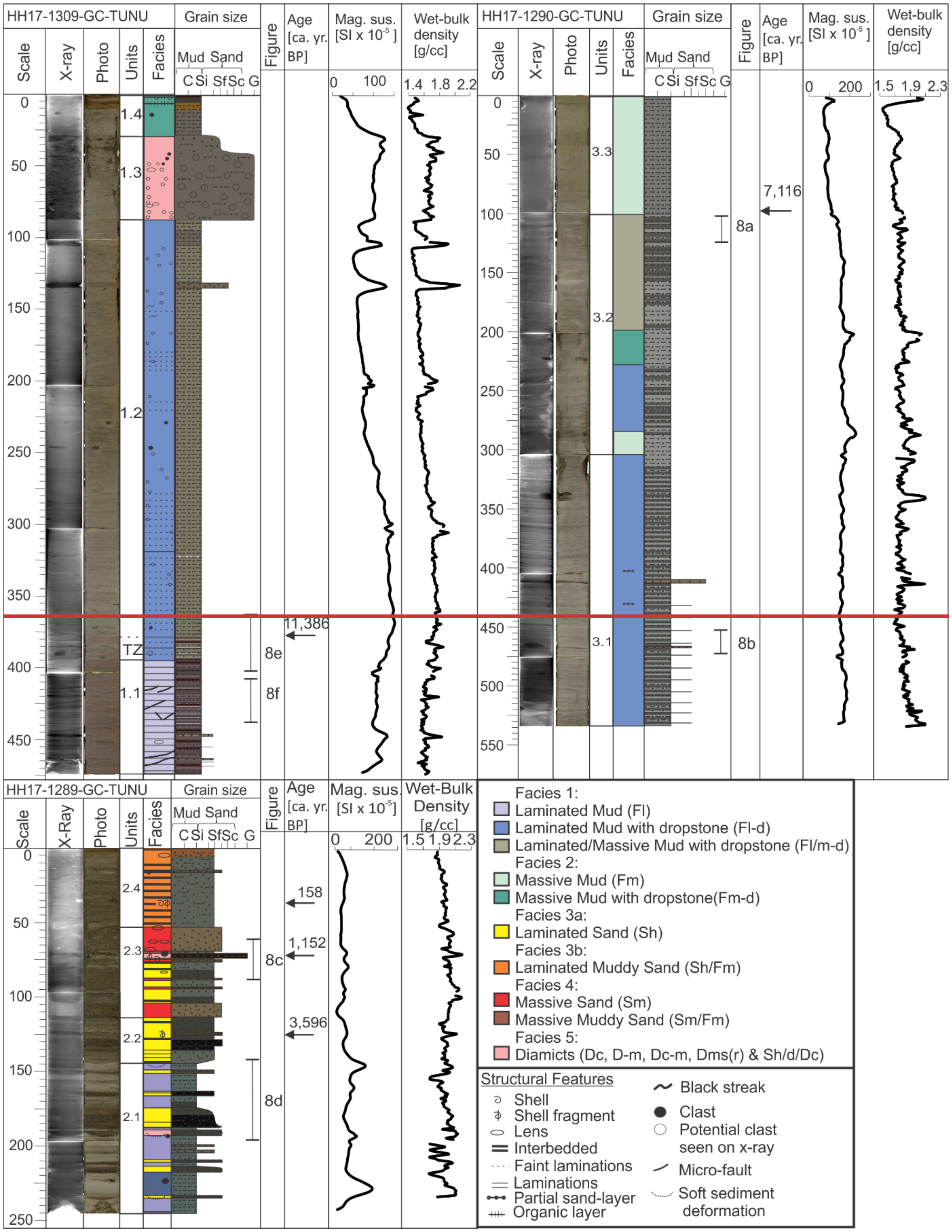

HH17-1309-GC-TUNU
Scale
X-ray
Photo
Units
Facies
Grain size
Mud Sand
C Si Sf Sc G
Figure
Age [ca. yr. BP]
Mag. sus. [SI x 10-5]
Wet-bulk density [g/cc]
1.4
1.3
1.2
TZ
1.1
11,386
8e
8f
HH17-1290-GC-TUNU
3.3
3.2
3.1
8a
8b
7,116
HH17-1289-GC-TUNU
2.4
2.3
2.2
2.1
158
1,152
3,596
8c
8d
Facies 1:
Laminated Mud (Fl)
Laminated Mud with dropstone (Fl-d)
Laminated/Massive Mud with dropstone (Fl/m-d)
Facies 2:
Massive Mud (Fm)
Massive Mud with dropstone(Fm-d)
Facies 3a:
Laminated Sand (Sh)
Facies 3b:
Laminated Muddy Sand (Sh/Fm)
Facies 4:
Massive Sand (Sm)
Massive Muddy Sand (Sm/Fm)
Facies 5:
Diamicts (Dc, D-m, Dc-m, Dms(r) & Sh/d/Dc)
Structural Features
Shell
Shell fragment
Lens
Interbedded
Faint laminations
Laminations
Partial sand-layer
Organic layer
Black streak
Clast
Potential clast seen on x-ray
Micro-fault
Soft sediment deformation

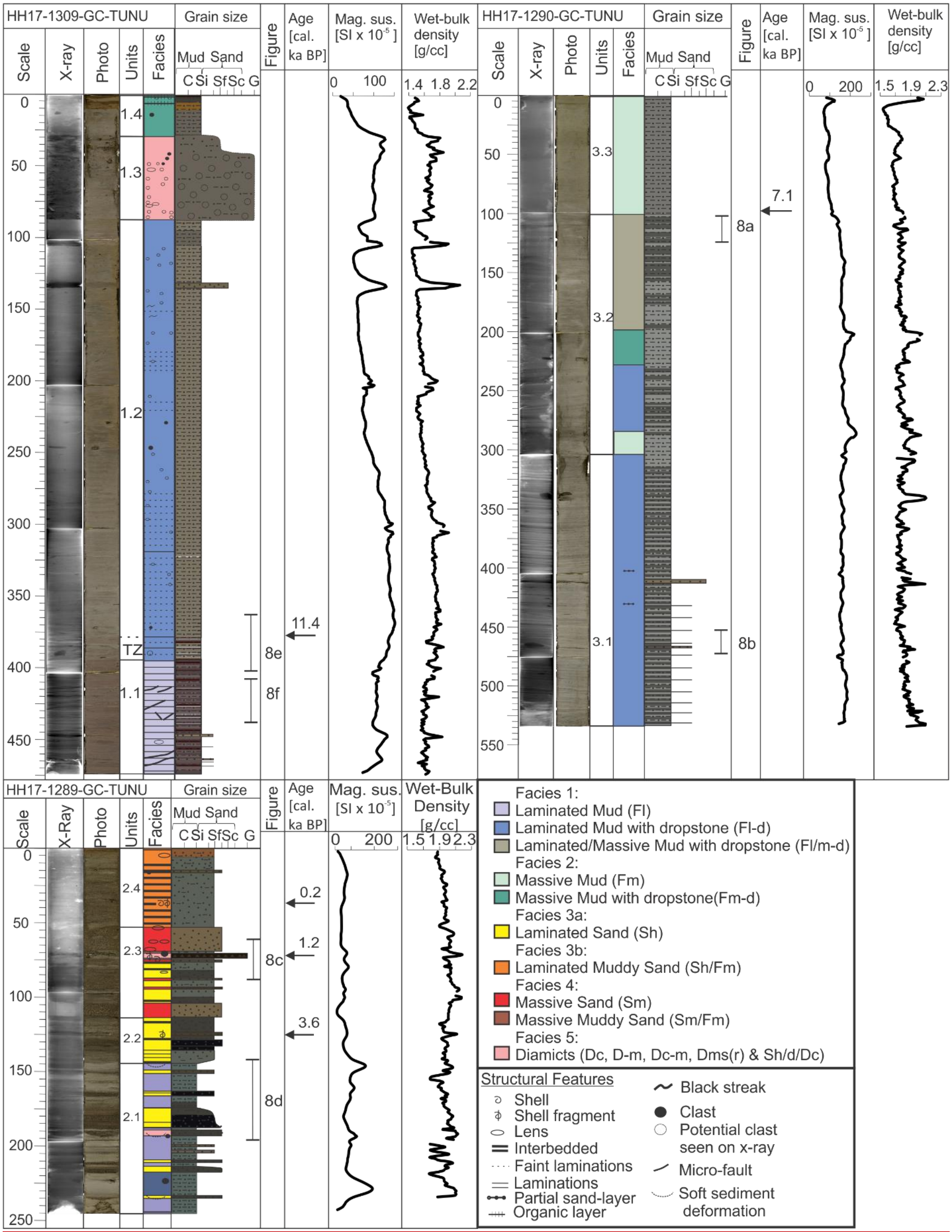
HH17-1309-GC-TUNU
Grain size
Scale
X-ray
Photo
Units
Facies
Mud Sand
C Si Sf Sc G
Figure
Age [cal. ka BP]
Mag. sus. [SI x 10^{-5}]
Wet-bulk density [g/cc]
1.4
1.3
1.2
TZ
1.1
11.4
8e
8f
HH17-1290-GC-TUNU
3.3
3.2
3.1
7.1
8a
8b
HH17-1289-GC-TUNU
X-Ray
Wet-Bulk Density [g/cc]
2.4
2.3
2.2
2.1
0.2
1.2
3.6
8c
8d
Facies 1:
Laminated Mud (Fl)
Laminated Mud with dropstone (Fl-d)
Laminated/Massive Mud with dropstone (Fl/m-d)
Facies 2:
Massive Mud (Fm)
Massive Mud with dropstone(Fm-d)
Facies 3a:
Laminated Sand (Sh)
Facies 3b:
Laminated Muddy Sand (Sh/Fm)
Facies 4:
Massive Sand (Sm)
Massive Muddy Sand (Sm/Fm)
Facies 5:
Diamicts (Dc, D-m, Dc-m, Dms(r) & Sh/d/Dc)
Structural Features
Shell
Shell fragment
Lens
Interbedded
Faint laminations
Laminations
Partial sand-layer
Organic layer
Black streak
Clast
Potential clast seen on x-ray
Micro-fault
Soft sediment deformation

Figure 7. Lithological core logs of the three gravity cores with x-ray images, core photos, unit divisions, facies, structures, magnetic susceptibility and wet-bulk density. TZ in HH17-1309-GC-TUNU stands for "Transition Zone". Grain size abbreviations: C: clay, Si: silt, Sf: fine grained sand, Sc: coarse grained sand and G: gravel.

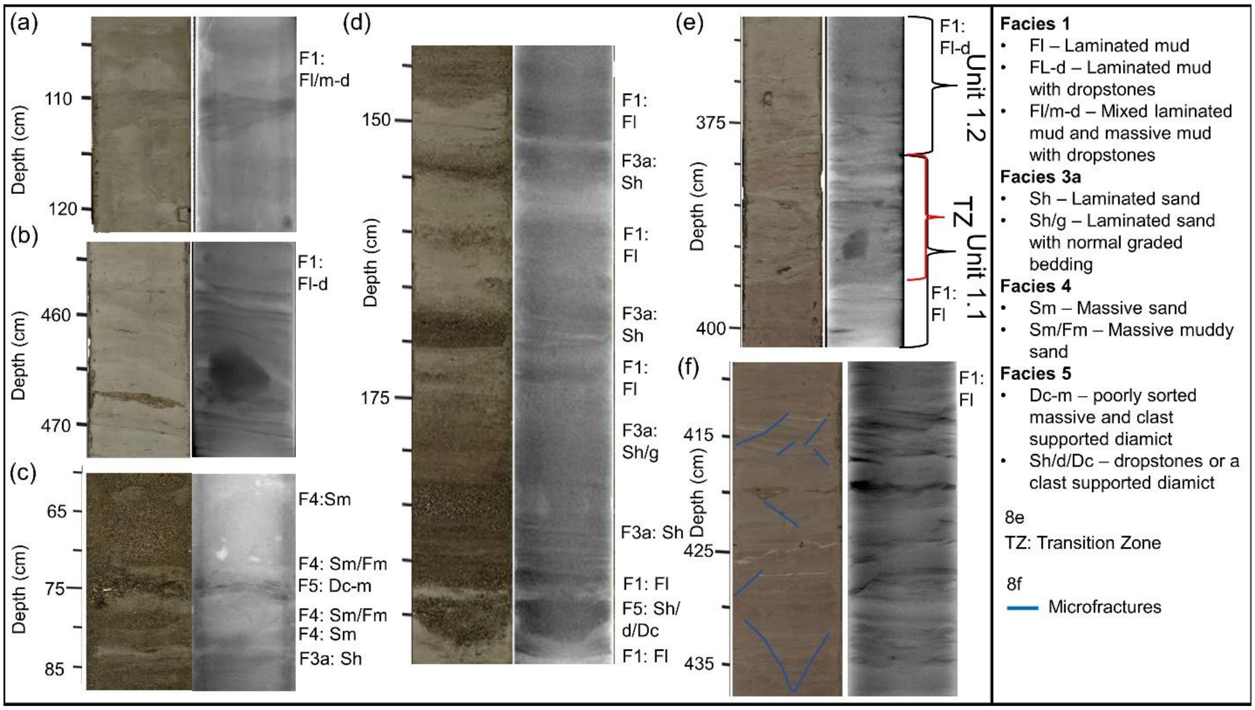

Figure 8. Photographic and x-ray images of sections of the three gravity cores (a-f). Corresponding facies codes can be found to the right of each image.

from turbid meltwater plumes in an ice-proximal environment (Evans et al., 2002). Large clasts have been interpreted as ice rafted debris (IRD). The formation of microfractures may have been caused by soft sediment deformation, possibly from grounded icebergs.

Facies 2 – Massive Mud (Fm & Fm-d)

The second facies consists of massive mud with or without dropstones and can be found in the inner fjord core HH17-1290 and the Store Bæ~~ae~~lt core HH17-1309 (Fig. 7). In HH17-1290 this appears downcore between sections of Facies 1 as well as in the topmost unit, Unit 3.3. The magnetic susceptibility gradually increases downcore in this facies in Unit 3.3. Further down core, in Unit 3.2, this facies is associated with a downwards trend in magnetic susceptivity following peaks in measured readings. Wet bulk density values roughly mirror these trends. In HH17-1309 massive mud units have been observed in Unit 1.4, where magnetic susceptibility and wet bulk density values increase downcore.

This facies is interpreted as being the result of suspension settling from overflow plumes and is believed to have been deposited in an ice-distal glacimarine environment with varying input from IRD (i.e., Boulton & Deynoux, 1981). Sediment may be sourced from a single location (i.e., Soranerbræen) or more than one location (e.g., local ice caps) in an ice-distal glacimarine environment with limited iceberg or sea-ice rafting. Massive mud deposits have also been identified in other Greenland fjords (e.g., Ó Cofaigh et al., 2001) and it has been suggested that they may indicate meltwater from ice- or fjord margin-distal conditions (Evans et al., 2002).

Facies 3a – Laminated Sand (Sh)

Facies 3a consists of sections of sand with horizontal sand laminations. This facies has been predominantly observed in the mid-fjord core, HH17-1289-GC-TUNU (Figs. 7 & 8d). These sections consist of fine to medium grained sand that range in thickness and colors. Occasionally this facies also contains normal graded bedding (e.g., Fig. 8d, ~174-183 cm). This facies does not contain uniform magnetic susceptibly or wet-bulk density readings as it has been found in association with low and high peaks of both parameters as well as values that are near the average for the core.

This facies is interpreted as being deposited from turbidity currents, possibly underflows that are either sourced from glacial or non-glacial streams and slope failures. Uniform layers may indicate a single, rapid event, where shifts in grain size and color may be the result of short-lived fluctuations in sediment input. Laminated sands have been identified in Scoresby Sund in East Greenland and have also been attributed to turbidite formation (Ó Cofaigh et al., 2001).

Facies 3b – Laminated Muddy Sand (Sh/Fm)

Facies 3b represents sections of sand with faint horizontal laminations as well as a large quantity of clay material interspersed throughout with faint laminations. This has been observed in HH17-1289 at the topmost unit in the core, Unit 2.4 (Fig. 7). Magnetic susceptibility is relatively uniform in this facies, where the wet-bulk density tends to decrease up core. Sediment grain size analysis of a single sample from this facies revealed that the sediment is composed of 56.3% sand and 43.7% mud. A "patch" of black organic material (i.e., plant material and shells) was also identified within this unit.

This complex facies is believed to have formed predominantly from underflow events, sandy – muddy turbidites, alternatively sandy turbidites with additional input from suspension settling. Similar deposits have been observed in Balsfjord, Norway although without lamination and possibly a higher mud content (Forwick and Vorren, 1998).

Facies 4 – Massive Sand / Massive Muddy Sand (Sm & Sm/Fm)

Facies 4 contains sections of massive sand (Sm) as well as massive sand with a large amount of clay content (Sm/Fm). This facies is predominantly found in Unit 2.3 (and to a much less extent, Unit 2.4) in HH17-1289 (Fig. 7). Sections of massive sand have been found in association with mud lenses and often contain horizontal sand layers (Sh) above and below it. Slight increases and decreases in magnetic susceptibility values have been observed within this facies.

This facies is believed to have developed through rapid deposition as well as deformation of Facies 3a & b. According to this interpretation, the mud lenses observed in this facies were once layers/lamina that became deformed due to the sand – mud density contrast. Massive sand has been found in Kangerlussuaq and Miki Fjords in East Greenland (Smith and Andrews, 2000) and well-sorted coarse grain deposits have been recovered near Petermann Glacier in northern Greenland (Reilly et al., 2019). Authors have attributed these layers to sediment gravity flows.

Facies 5 – Diamicts (Dc, D-m, Dc-m, Dms(r) & Sh/d/Dc)

Facies 6 contains a variety of different diamicts observed within the mid-fjord core HH17-1289 and the Store Bæ~~ae~~lt core HH17-1309. In HH17-1289 this includes a 3.5 cm poorly sorted massive and clast supported diamict (Dc-m) in the middle of Unit 2.3 (Figs. 7 & 8c), and a horizontally laminated layer of sand that that is either accompanied by dropstones or a clast supported diamict (Sh/d/Dc) (Figs. 7 & 8d). It is inferred that they are the result of sea ice or iceberg rafting/dumping. Within HH17-1309 there is a substantially larger, sharp based, matrix-supported diamict, stratified in its upper part (Dms(r)) in Unit 1.3 (Fig. 7). Based on these characteristics, this diamict has been interpreted as a density flow deposit, likely a debris flow deposit that is overlain by (part of) a turbidite.

4.3.2. Core chronology ~~and sedimentation rates~~

Shell and shell fragments were recovered from HH17-1289 for radiocarbon dating. At 34 cm depth, a semi-spherical path of organic content was identified, containing two intact *Yoldiella lenticula*, a shell fragment and plant material. Additionally, at 71 cm depth, a large 3 cm half of a *Hiatella arctica* shell was collected for dating, and shell fragments were recovered from a depth of 125 cm for the same purpose. These shells yielded radiocarbon ages of 0.2~~158~~, 1.2~~,152~~ and 3.6~~,596~~ cal. ka~~yr.~~ BP, respectively (Table 5).

Cores HH17-1290 and HH17-1309 were subsampled for foraminifera material at four positions~~.~~ and ~~C~~calcareous benthic species~~, which were rare,~~ were used for dating. In HH17-1290 this ~~and~~ included predominantly *Melonis barleeanus* ~~as well as~~and small amounts of *Islandiella norcrossi*~~, but in substantially smaller quantities~~. In HH17-1309, at a depth of 377 cm *Islandiella norcrossi* (rare to common), ~~&~~ *Stainforthia feylingi* (rare) and a planktonic species were identified immediately above the transition zone between two facies. ~~deformed (below) and undeformed sediments (above).~~ Radiocarbon dates for the HH17-1309 sample yielded an age of 11.4~~,386~~ cal. ka~~yr.~~ BP where the sample from HH17-1290 yielded an age of 7.1~~,116~~ cal. ka~~yr.~~ BP (Table 5).

Table 5. Calibrated ~~R~~radiocarbon dates~~, calibrated dates, and associated linear sedimentation rates.~~ using the online version of OxCal 4.4 and the Marine20 calibration curve (Heaton et al., 2020),

Coring station	Sampling Depth [cm]	Lab nr.	Species	^{14}C age BP	Marine20 cal BP (1σ range)	Marine20 cal BP	Linear sedimentation interval [cm]	Linear sedimentation rate Marine20 [cm/ka]
HH17-1309-GC-TUNU	377	5157.1.1	Mixed benthic foraminifera	10357 ± 95	11201 - 11553	11386	0-377	33.11
HH17-1289-GC-TUNU	35	5154.1.1	*Yoldiella lenticula*	688 ± 34	61 - 253	158	0-35	221.52
HH17-1289-GC-TUNU	71	5155.1.1	*Hiatella arctica*	1747 ± 28	1065 - 1250	1152	35-71	31.25
HH17-1289-GC-TUNU	125.5	5156.1.1	Bivalve frag.	3809 ± 36	3472 - 3701	3596	71-125.5	15.16
HH17-1290-GC-TUNU	97	5158.1.1	Mixed benthic foraminifera	6800 ± 80	6990-7250	7116	0-97	13.63

Coring station	Sampling Depth [cm]	Lab nr.	Species	^{14}C age BP	Marine20 cal BP (1σ range)	Marine20 cal BP
HH17-1309-GC-TUNU	377	5157.1.1	Mixed benthic foraminifera	10357 ± 95	11201 - 11553	11386
HH17-1289-GC-TUNU	35	5154.1.1	*Yoldiella lenticula*	688 ± 34	61 - 253	158
HH17-1289-GC-TUNU	71	5155.1.1	*Hiatella arctica*	1747 ± 28	1065 - 1250	1152
HH17-1289-GC-TUNU	125.5	5156.1.1	Bivalve frag.	3809 ± 36	3472 - 3701	3596
HH17-1290-GC-TUNU	97	5158.1.1	Mixed benthic foraminifera	6800 ± 80	6990-7250	7116

~~Linear sedimentation rates were calculated assuming modern sediments are at the core top as no overpenetration was recorded during the sampling of these cores and that during the core logging little sediment disturbance was found (Table 5). Given the scarcity of biological material in these cores these sedimentation rates act only as a first approximation until a more detailed record can be recovered. Using the available (calibrated) dating results, sedimentation rates of ~15 cm/ka, ~31 cm/ka, & ~222 cm/ka were calculated for core HH17-1289 at 71-125.5 cm, 35-71 cm, and 0-35 cm, respectively. These results reveal an increase in the sedimentation rate towards the present. However, as this core includes multiple deposits from turbidity currents (i.e., reworked deposits), linear sedimentation rates in core HH17-1289 should be treated with caution. An average, linear rate of ~14 cm/ka was calculated for the interval of 0-97 cm in core HH17-1290 and an average, linear rate of ~33 cm/ka was also obtained for the large interval of 0-377 cm in core HH17-1309. These linear rates are lower, up to an order of magnitude, when compared to the Kejser Franz Josef Fjord system ~400 km south of the study area (Olsen et al., 2022). The origin of this observed difference must await further studies.~~

5. Discussion

5.1. Ice Sheet advance

The appearance of glacial lineations in Bessel Fjord suggest that the fjord was once fully glaciated, which is in accordance with the inferred shelf break-terminating ice sheet inferred for the LGM from other studies (e.g., Laberg et al., 2017; Olsen et al., 2020) (Figs. 9a & 9b). Ice that filled the fjord is believed to most likely be from the modern Soranerbræen glacier but may have also included ice caps and other nearby branches of inland ice.

Glacial lineations are believed to have formed during the LGM but could have also formed during an ice readvance in the deglaciation (see below). Onshore and south of Bessel Fjord, two sets of striations identified in Langsødalen (Hjort, 1979, 1981) may suggest that this valley experienced two glaciation events (Fig. 1c). Striations, and lateral moraines, found along the fjord axis may be the result of the east-west movement of ice through the valley, where SW oriented striations may be the result of Storstrømmen encroaching also onto terrestrial areas. Hjort (1981) suggested that striae on Haystack may indicate that ice flow was dominant from the north during the Nanok Stadial but ice pressure from Langsødalen dominated later after deglaciation begun. Thus, it is possible that ice masses drained through both Bessel Fjord and Langsødalen during full-glacial conditions further advancing into Dove Bugt/Store Bælt.

In Store Bælt, the orientation of glacial lineations (e.g., MSGLs) suggest that ice flowed to the south along the west cost of Store Koldewey, marking the southwards expansion of the Storstrømmen ice stream (Figs. 9a & 9b). East of Dove Bugt, MSGLs identified in Store Koldewey Trough are believed to have formed when the Storstrømmen ice stream acted as a "pure" ice stream (Bentley, 1987; Stokes and Clark, 1999) and overrode the underlying topography during the LGM (Fig. 9a; Olsen et al., 2020). It was theorized that at a later phase, when the ice sheet began to thin, the ice stream became more influenced by the topography of deep troughs, draining northwards to Jøkelbugten and southwards to Dove Bugt (Olsen et al., 2020). Assuming these two phases occurred in the Storstrømmen ice stream development, it is possible that these glacial lineations in Store Bælt represent a period when a branch of the ice stream began conforming to topographical controls (e.g., Store Koldewey) and flowed towards the south. At this point the ice may have flowed into the southeast through Dove Bugt Trough (Fig. 9a).

An alternative interpretation, that cannot be excluded, is that these MSGLs formed during a glacial re-advance that followed the LGM. Between Hochstetter Forland and Shannon Ø a submerged moraine has been identified in Shannon Sound, which may indicate that at one point the ice stream travelled south rather than through Dove Bugt Trough (Figs. 9b & 10a; Hjort, 1981; Landvik, 1994; Larsen et al., 2016; Funder et al., 2021). However, constraints from ~~onshore deglaciation ages in~~ Store Koldewey, Germania Land and Trums Ø, do not support an ice advance during the Younger Dryas (Fig. 10b; see below). ~~This~~The formation of the submerged moraine was possibly due to an ice readvance of the GrIS outlet(s) (Soranerbræen, L. Bistrup Bræ and/or Storstrømmen) through western, inner Dove

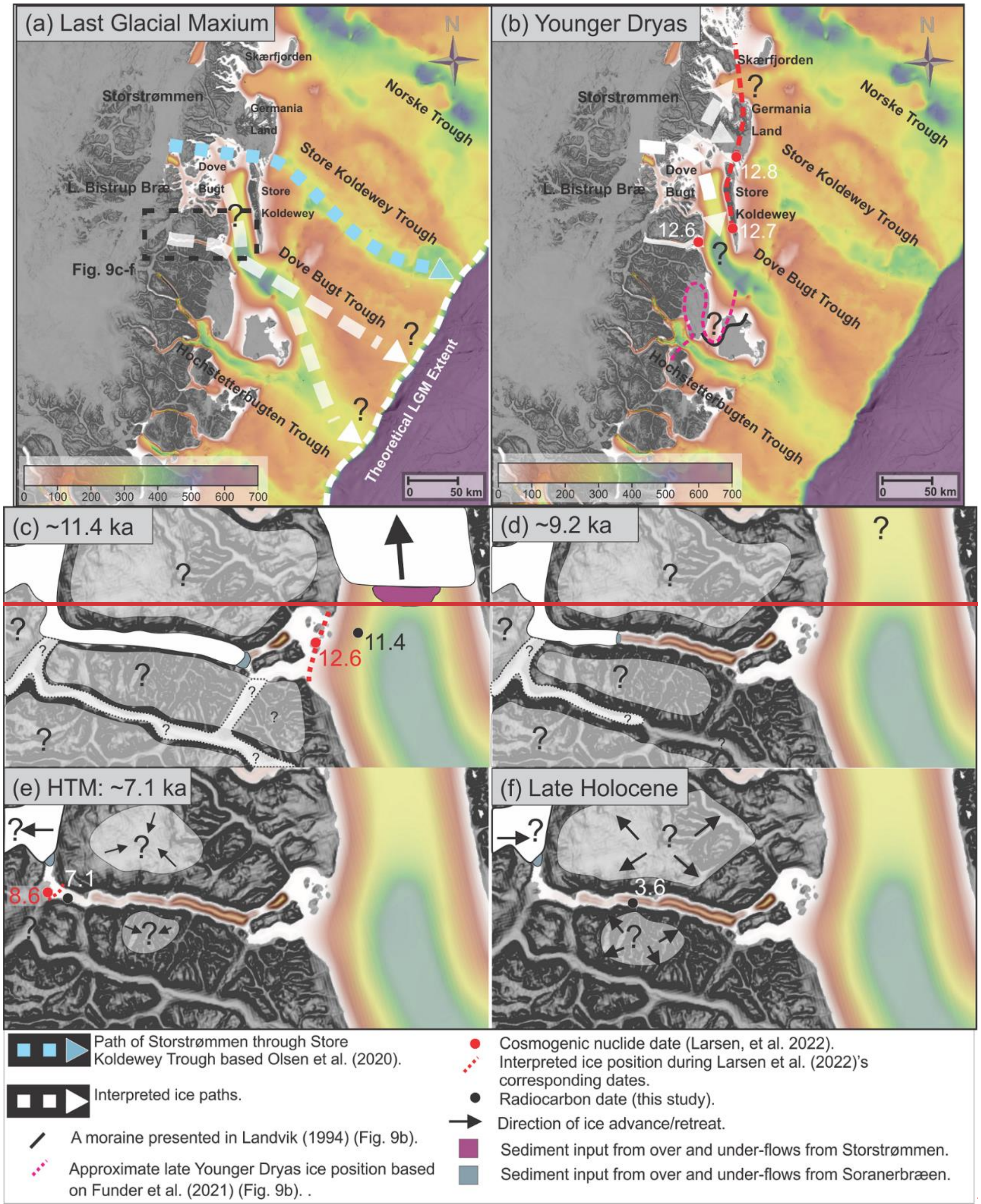

(a) Last Glacial Maxium
(b) Younger Dryas
N
Skærfjorden
Storstrømmen
Germania
Land
Norske Trough
Dove
Bugt
Store
Koldewey
Store Koldewey Trough
L. Bistrup Bræ
Fig. 9c-f
Dove Bugt Trough
Hochstetterbugten Trough
Theoretical LGM Extent
12.8
12.6
12.7
0 100 200 300 400 500 600 700
0 50 km
(c) ~11.4 ka
(d) ~9.2 ka
(e) HTM: ~7.1 ka
(f) Late Holocene
11.4
12.6
8.6
7.1
3.6
Path of Storstrømmen through Store Koldewey Trough based Olsen et al. (2020).
Interpreted ice paths.
A moraine presented in Landvik (1994) (Fig. 9b).
Approximate late Younger Dryas ice position based on Funder et al. (2021) (Fig. 9b). .
Cosmogenic nuclide date (Larsen, et al. 2022).
Interpreted ice position during Larsen et al. (2022)'s corresponding dates.
Radiocarbon date (this study).
Direction of ice advance/retreat.
Sediment input from over and under-flows from Storstrømmen.
Sediment input from over and under-flows from Soranerbræen.

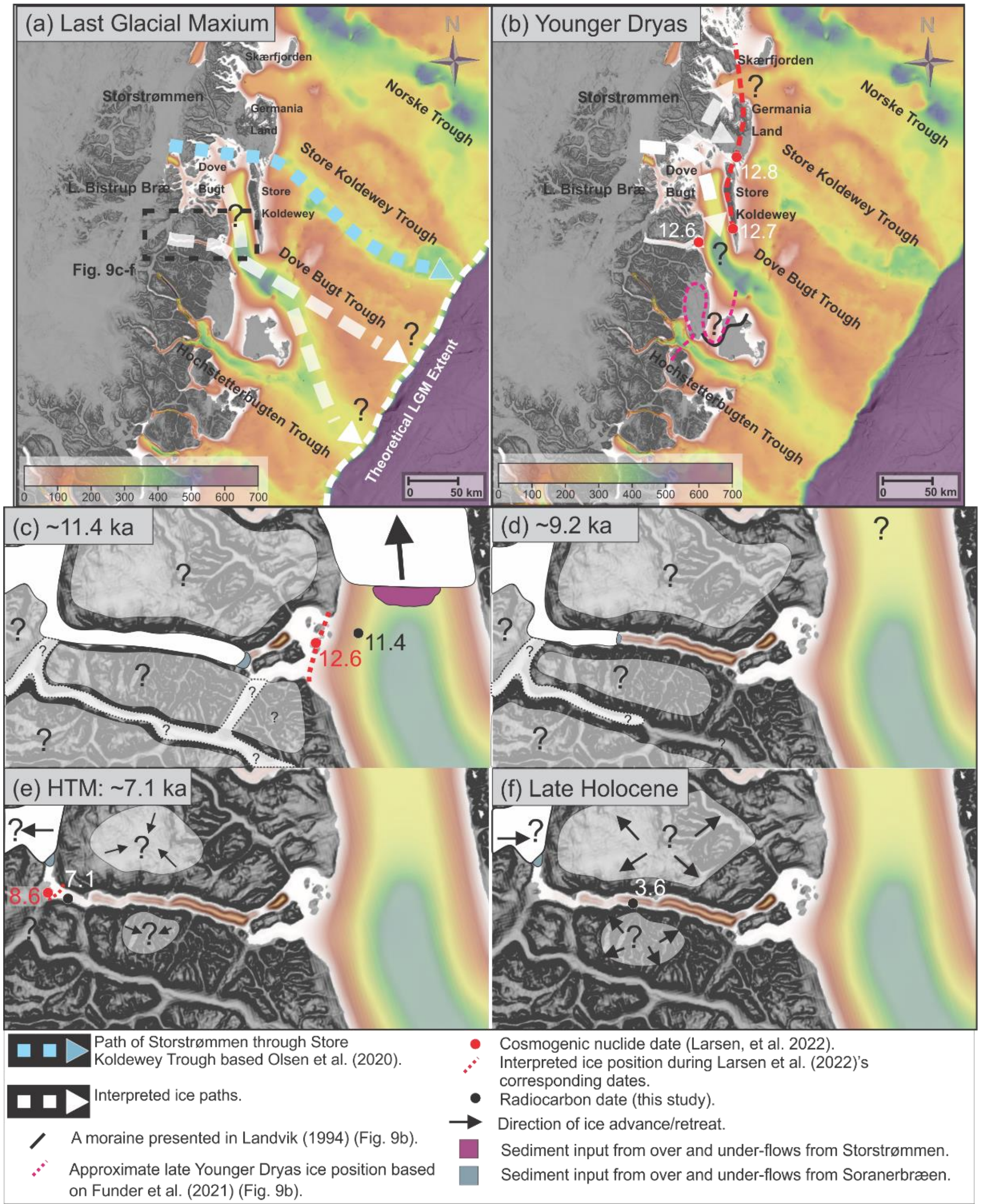

Figure 9. Maps showing ice sheet extent and advancement/retreat directions in SW Dove Bugt and Bessel Fjord during a range of periods. (a) The interpreted position of the ice sheet during the LGM. (b) The theoretical position of ice in Bessel Fjord and Dove Bugt during the Younger Dryas. (c) The ice position in Bessel Fjord at ~11.4 ka based on approximated deglaciation date presented in this study and the position and radiocarbon date for gravity core HH17-1309. The size of ice caps in c-f are only indicative. (d) The position of ice in Bessel Fjord at ~9.2 ka based on approximated deglaciation data from this study. (e) Ice retreating beyond our gravity core (HH17-1290) at ~7.1 ka during the HTM. (f) The Late Holocene ice expanse in Bessel Fjord with a radiocarbon date from gravity core HH17-1289. Background bathymetry displayed using IBCAO data (Jakobsson et al., 2020).

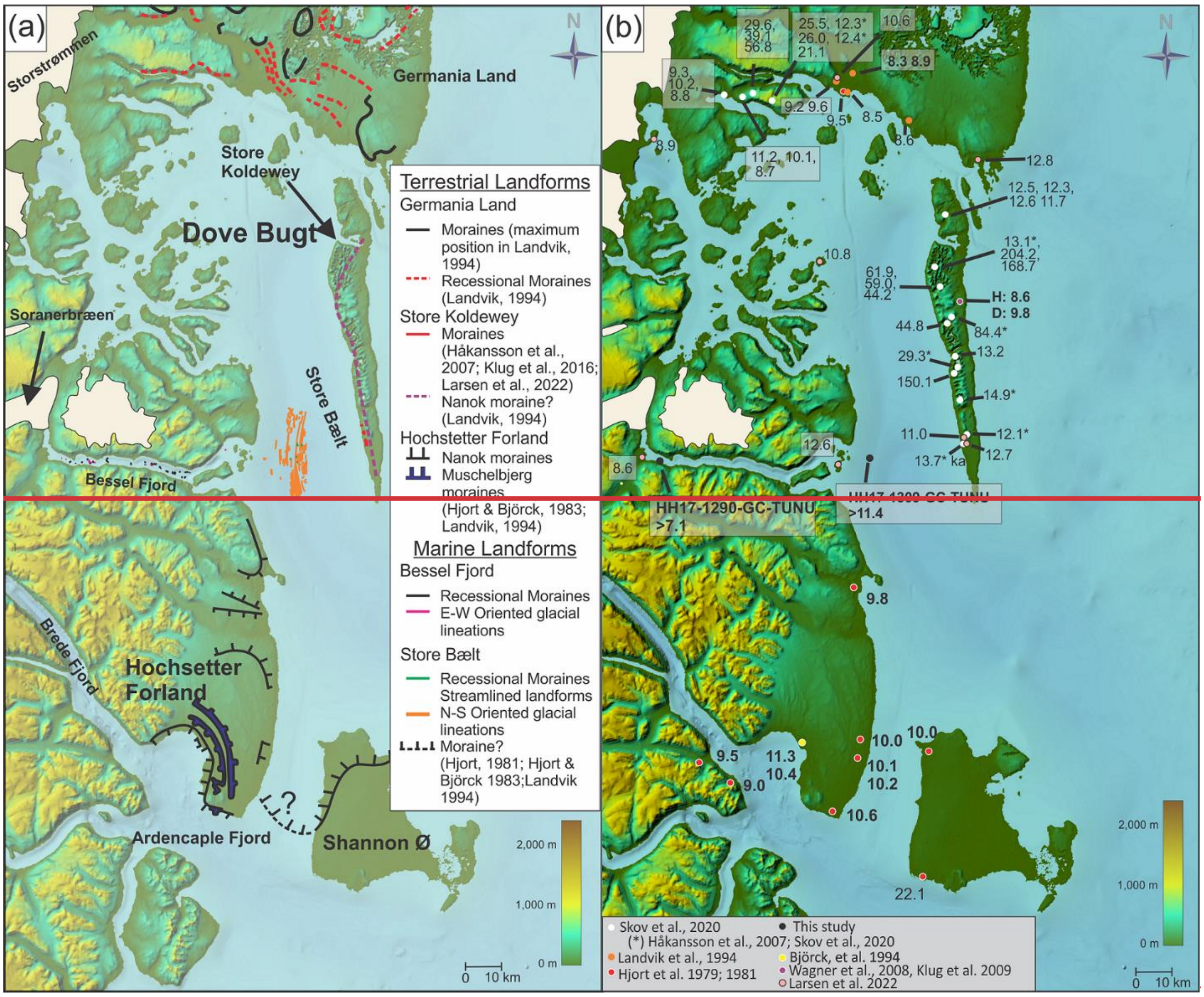

(a)
Storstrømmen
Germania Land
Store Koldewey
Dove Bugt
Soranerbræen
Store Bælt
Bessel Fjord
Brede Fjord
Hochsetter Forland
Ardencaple Fjord
Shannon Ø
Terrestrial Landforms
Germania Land
Moraines (maximum position in Landvik, 1994)
Recessional Moraines (Landvik, 1994)
Store Koldewey
Moraines (Håkansson et al., 2007; Klug et al., 2016; Larsen et al., 2022)
Nanok moraine? (Landvik, 1994)
Hochstetter Forland
Nanok moraines
Muschelbjerg moraines
(Hjort & Björck, 1983; Landvik, 1994)
Marine Landforms
Bessel Fjord
Recessional Moraines
E-W Oriented glacial lineations
Store Bælt
Recessional Moraines
Streamlined landforms
N-S Oriented glacial lineations
Moraine? (Hjort, 1981; Hjort & Björck 1983;Landvik 1994)
2,000 m
1,000 m
0 m
0 10 km
(b)
29.6, 39.1 56.8
25.5, 12.3* 26.0, 12.4* 21.1
10.6
8.3 8.9
9.3, 10.2, 8.8
9.2 9.6
9.5
8.5
8.6
8.9
11.2, 10.1, 8.7
12.8
12.5, 12.3, 12.6 11.7
10.8
13.1*, 204.2, 168.7
61.9, 59.0, 44.2
H: 8.6
D: 9.8
44.8
84.4*
29.3*
13.2
150.1
14.9*
11.0
12.1*
13.7* ka
12.7
12.6
8.6
HH17-1290-GC-TUNU >7.1
HH17-1300-GC-TUNU >11.4
9.8
10.0
10.0
11.3
10.4
10.1
10.2
9.5
9.0
10.6
22.1
Skov et al., 2020
(*) Håkansson et al., 2007; Skov et al., 2020
Landvik et al., 1994
Hjort et al. 1979; 1981
This study
Björck, et al. 1994
Wagner et al., 2008, Klug et al. 2009
Larsen et al. 2022
2,000 m
1,000 m
0 m
0 10 km

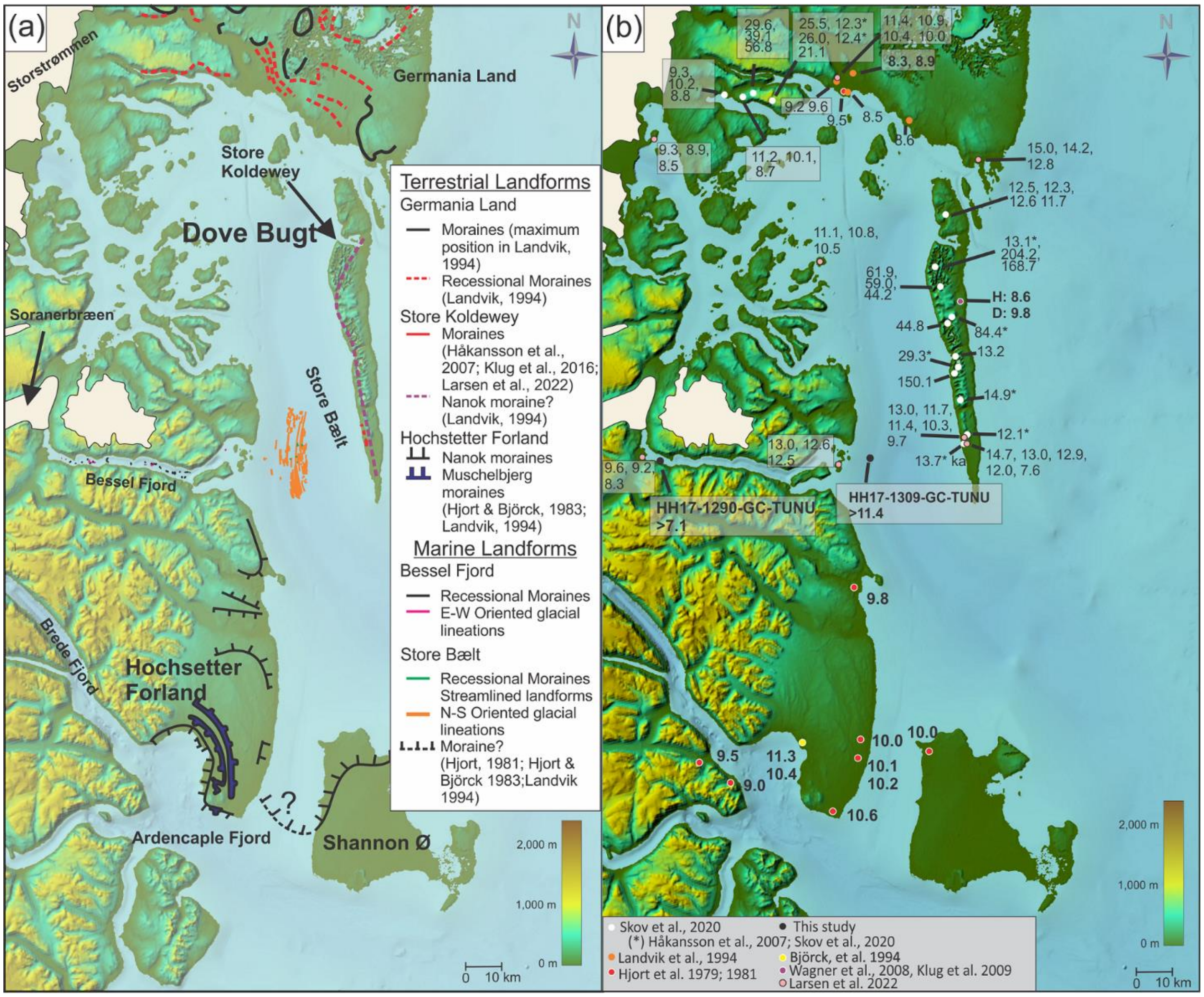

Figure 10. (a) Marine moraine ridges and glacial lineations from the current study together with previously mapped marine and terrestrial features. (b) Location of deglaciation dates from this study (Table 5) and previous publications. See Table 3 for recalibrated radiocarbon dates. H: Hjort Lake, D: Duck Lake. Background displayed using IBCAO data (Jakobsson et al., 2020).

Bugt (Fig. 9b), where the surroundings (onshore and offshore) were not or less affected. If this is correct, the readvance may have occurred during the Younger Dryas (prior to 11.4 ~~ka~~ cal. ka BP, see below).

5.2. Ice Sheet retreat through Store Bælt

The deglaciation age of 11.4 ~~ka~~ cal. ka BP (Table 5) from Store Bælt immediately east of the Bessel fjord entrance is attributed to the retreat of a N-S bound branch of the NEGIS (Fig. 9c) due to the presence of N-S oriented glacial lineations near the gravity core. This date represents a minimum age for the deglaciation as it is not from the base of the deglacial deposits. Previously published dates constraining the timing of deglaciation in Dove Bugt have been restricted to terrestrial regions (Fig. 10b). Using cosmogenic nuclide dating, Skov et al., (2020) produced deglaciation ages of ca. 12.7 ka ~~cal BP~~ at Store Koldewey and ca. 9.8 ka ~~cal BP~~ at Pusterdal and later Larsen et al. (2022) produced a number of deglaciation ages across Dove Bugt and Bessel Fjord (8.6-12.8 ka ~~cal BP~~) (Fig. 10b).

Our minimum age of ~11.4 ~~ka~~ cal. ka BP from HH17-1309 largely matches findings in Dove Bugt and Hochstetter Forland (Fig. 10b). It is slightly later than average cosmogenic nuclide ages obtained from Larsen et al. (2022) on Trums Ø (12.6 ka ~~cal BP~~) and a Nanok moraine on southern Store Koldewey (12.7 ka ~~cal BP~~), but earlier than a second Store Koldewey Nanok moraine (11.0 ka ~~cal BP~~) as well as positions closer to the modern ice margin of Storstrømmen, such as Licht Ø (10.8 ka ~~cal BP~~) and Bræ Øerne (8.9 ka ~~cal BP~~). Thus, Store Koldewey, and Trums Ø may have been partially deglaciated slightly prior to the final retreat of the NEGIS through Store Bælt.

Radiocarbon dates obtained from lake sediments on Store Koldewey suggest that the earliest onset of warmth may have begun ~10 ~~ka~~ cal. ka BP (Klug et al., 2009), therefore, the deglaciation of the area beginning prior to this may further support these results. Additionally, Landvik (1994) produced a range of deglaciation ages between 9.6 to 8.5 ~~ka~~ cal. ka BP along the northern coast of Dove Bugt (Hvalrosodden and Snenæs on Germania Land) and Hjort (1981, 1979) provided a range of delegation ages between 10.6 to 9.8 ~~ka~~ cal. ka BP on Hochstetter Forland. Later Björck et al. (1994), on Hochstetter Forland, dated *Hiatella arctica* shells near the shore of Peters Bugt Sø and *Portlandia arctica* shells in a delta distal to a Nanok I ridge to 10.4 and 11.3 ~~ka~~ cal. ka BP, respectively (Table 3; Fig. 10b).

Although based on a limited data set, the lack of prominent morainal landforms in Store Bælt may also suggest a rapid retreat through the region. A small number of retreat moraines have been observed in an isolated region of the study area, but the most prominent geomorphic landforms are glacial lineations. Placing Store Bælt within the context of Dowdeswell et al. (2008)'s proposed model for ice streams in high latitudes, ice likely retreated through the area rapidly, although the presence of small moraines may suggest brief periods of stagnation. This is in accordance with findings by Larsen et al. (2020, 2022) that deep fjords and outer regions in eastern North Greenland were rapidly deglaciated between ~12.6 and 10 ka ~~cal BP~~. However, additional data is required to confirm this.

Oceanic warming is believed to have contributed to the deglaciation of the inner shelf further north and south of Dove Bugt (e.g., Jackson et al., 2022; Davies et al., 2022). Within the study area, Store Koldewey does largely block oceanic water from the shelf from entering Store Bælt, however, it is possible that warmer water traveled through the Dove Bugt Trough to the south and impacted a north-south branch of the ice stream. This mechanism for warm water transport has also been suggested for other east Greenland troughs (Arndt et al., 2015) and used to explain how warm water has reached other outlets of the NEGIS (e.g., Zachariae Isstrøm via the Norske Trough (Schaffer et al., 2017)).

5.3. Ice ~~S~~sheet retreat through Bessel Fjord

Cosmogenic nuclide dates from Trums Ø suggest that the deglaciation of the outer fjord began around 12.6 ka (Larsen et al., 2022) ~~cal BP~~. Gravity core HH17-1290, collected from the inner fjord region, consists of sediments that reflect an increasingly ice distal environment up core. One radiocarbon date from the core provides a minimum age of ~7.1 ~~ka~~ cal. ka BP for the deglaciation of Soranerbræen and/or local ice caps from the inner fjord region (Table 5 & Fig. 9e). This date, however, is not from the base of the deglacial deposits and therefore represents a minimum age for the deglaciation of the inner fjord. New cosmogenic nuclide dates from Vandrepasset (onshore innermost Bessel fjord area, connecting the fjord and the next valley to the south) provide an age of 8.6 ka ~~cal BP~~ for the deglaciation of the innermost fjord area (Larsen et al., 2022), confirming this interpretation. Our minimum age of 7.1 ~~ka~~ cal. ka BP and the results of Larsen (2022) falls within a modelled ice sheet extent by Lecavalier et al. (2014) which placed the position of the ice sheet in the middle of Bessel Fjord at 9 ~~ka~~ cal. ka BP and that the present-day ice margin is reached by 6 ~~ka~~ cal. ka BP. The minimum age also agrees with the onset of HTM on Store Koldewey (~8.0 to 4.0 ~~ka~~ cal. ka BP) (Wagner et al., 2008; Klug et al., 2009; Schmidt et al., 2011) and Hochstetter Forland (8.8 and 5.6 ~~ka~~ cal. Ka BP) (Björck & Persson, 1981; Björck et al., 1994). Thus, the GrIS retreated from the marine realm in ~~e~~Early Holocene, slightly before or at the time of the HTM in this region (characterized by a mean July temperature 2-3°C higher than at present; Bennike et al., 2008).

The appearance of recessional moraines in Bessel Fjord suggests that the fjord underwent a stepwise deglaciation. The large moraine identified between Basin 3 and Basin 4 (M3; Fig. 7e) is believed to have formed during a major ice halt or readvance, possibly climatically induced. Smaller moraines occasionally follow topographic boundaries, which may suggest that the retreat of ice in Bessel Fjord was also partly topographically controlled. Recessional moraines identied by Olsen et al (2020) east of Dove Bugt in Store Koldewey Trough contain similar heights to those identified here (excluding M3). However, there are more moraines identified in Store Koldwey Trough than in Bessel Fjord, and they are wider, which is likely due to the lack of topographic confinment.

A decrease in atmospheric temperatures in early Holocene is recorded in the Greenland Summit temperature records and includes the Preboreal Oscillation~~,~~ and the 9.2 ka event ~~, the Pre-8.2 ka cooling, and the 8.2 ka event, with the 8.2 ka event being the largest hemispheric-wide negative temperature excursion during the Holocene~~ (Kobashi et al., 2017). We tentatively suggest that some of the moraines identified in the Bessel fjord may have developed during some of these events. From this we suggest that increased Northern Hemisphere summer insolation that peaked in the early Holocene was the main control for this part of the deglaciation during which the ice front receded from the coastline to the west of (onshore) Bessel Fjord, a distance of ~60 km. Assuming that this occurred over a maximum period of ~4.3 ~~ka~~ cal. ka BP (11.4-7.1 ~~ka~~ cal. ka BP, see discussion above on the timing and length of this period), this corresponds to an average minimum ice recession rate of ~14 m/yr. Further supporting this average rate, if one applies this same approach to the two average Bessel Fjord cosmogenic nuclide dates presented by Larsen et al. (2022) (12.6-8.6 ka) and the distance between their sampling locations (~56 km), it also results in a rate of 14 m/yr. This rate ~~, a minimum rate,~~ is considered realistic as it is half (or less) than the rate estimated from the Nioghalvfjerdsfjorden further north (also part of the Storstrømmen ice stream) where a rate of ~30-40 m/yr was reported (Bennike & Björck, 2002). This rate places Soranerbræen near the large moraine M3 around the 9.2 ka event (Fig. 9d).

~~Applying this minimum rate to the distance between Trums Ø (Larsen, et al., (2022); 12.6 ka cal BP) and the major mounds and moraines identified in this study (M1, M2, M3 & M6), yields the approximate minimum ages of 11.4, 10.5, 9.7 and 9.2 ka, respectively. This places Soranerbræen between large moraine M3 and the bedrock mound M6 around the 9.2 ka event (Fig. 9d). This is noteworthy as M3, and other many of the smaller moraines identified between these two features, may have formed during this climatically cooler period. Additionally, many smaller moraines in the fjord follow topographic boundaries, which may suggest that the retreat of ice in Bessel Fjord was partly topographically controlled.~~

While oceanic warming may be partially responsible for the retreat of the NEGIS through Store Bælt, we believe that Bessel Fjord is too sheltered by the sill at its entrance to have allowed warm, intermediate water to enter and make a significant impact of the deglaciation of the southern outlet of Soranerbræen. Our bathymetric dataset reveals that the depth of the sill is between ~50 to 200 m, however large parts of it are above water and form islands. This is far shallower than other fjord sills in the region that are theorized to have blocked warm Atlantic Water (e.g., the sill in Dijmphna Sund to the north, which has a maximum depth of 170 m (Wilson and Straneo, 2015)). Also, the effect of the glacio-eustatic readjustment is considered to be small for this region, ~9.5 m higher in the Young Sound region (slightly south of our study area) 7500 years ago (Pedersen et al., 2011). Rignot et al. (2022) also theorized that seafloor topography may impact whether warm water is reaching the northern outlet of Soranerbræen. They suggested further that the grounding line retreat of Storstrømmen, L. Bistrup Bræ,and possibly Soranerbræen, may primarily be caused by ice thinning from atmospheric warming (Rignot et al., 2022). We suggest that a similar mechanism may be responsible for Soranerbræen's retreat through Bessel fjord during the deglaciation.

5.4. Holocene glacier variability and sedimentary processes in Dove Bugt

Sedimentological evidence (e.g., ice-proximal laminated muds) from HH17-1309 suggests, that suspension settling from a glacial source(s) likely dominated southwestern Dove Bugt during the Holocene. The contribution of sediment from the NEGIS seems unlikely, as Pusterdal became deglaciated by 9.5 ka~~ cal BP~~ (Skov et al., 2020) and Storstrømmen retreated beyond Bræ Øerne by 8.9 ka ~~cal BP ~~(Larsen et al., 2022), therefore it very well may be from Soranerbræen, or local ice caps.

During the latter part of the HTM in the middle Holocene, a time period in which some glaciers are believed to have reached their minimum extent across Greenland, the NEGIS is believed to have retreated beyond its current position between 5.4 to 1.2 ~~ka ~~cal. ka BP (Table 3), creating the Storstrømmen Sound (Weidick et al., 1994). ~~Relating the core sedimentology to a linear age model developed from sedimentation rates (i.e., Table 5), l~~Laminations appear less frequently in the upper part of core HH17-1309 ~~during this period~~, yet they are not absent. Laminations are entirely absent in the Bessel Fjord core HH17-1290 during this period and remain absent through the colder Late Holocene. Later, during the Little Ice Age, Storstrømmen has demonstrated to have expanded to its modern day position (Weidick et al., 1994).

Gravity core HH17-1289, collected to the north of an onshore glaciofluvial channel connected to a modern-day ice cap, transitions to complex assortment of sand layers just prior to 3.6~~,596~~ cal. ~~yr~~ka BP (Fig. 7). Sedimentological evidence suggests that these sand layers are largely the result of rapid, short lived depositional events (i.e., turbidity currents) interpreted to be related to the growth of a delta slightly south of the core site, from glacifluvial sediment input from a nearby outlet glacier.

Pollen assemblage data from Hochstetter Forland mark the end of the HTM at 5.6 cal. ka~~yr~~ BP (Björck and Persson, 1981; Björck et al., 1994) and information derived from aquatic organisms mark the end of the HTM on Store Koldewey at 4 cal. ka~~yr~~ BP (Wagner et al., 2008; Klug et al., 2009b; Schmidt et al., 2011). This coincides with the onset of turbidites in core HH17-1289. Therefore, it is possible that this shift to sand dominated sedimentation within this core was controlled by climatically driven processes. This onset is here suggested to result from higher sediment input through the channel as local ice caps expanded outwards following the HTM, possibly in response to this climate cooling (Fig. 9f). This period of cooling also corresponds to extended concentrations of sea ice on the shelf (Kolling et al., 2017).

6. Conclusion

In summary:

- Glacial lineations (MSGLs) identified in SW Dove Bugt suggest fast-flowing ice, interpreted to be from the NEGIS, developed during the LGM or an ice readvance during the deglaciation.
- Our minimum deglaciation date for Store Bælt (>11.4 ~~ka~~ cal~~.p~~ ka BP) is slightly ~~later~~ younger than new cosmogenic nuclide dates found onshore on Trums Ø and one of two Nanok stadials on Store Koldewey (Larsen et al., 2022) as well as various other dates across Store Koldewey (e.g., Skov et al., 2020). Thus, Store Koldewey and Trums Ø may have been partially deglaciated prior to the final retreat of the NEGIS through Store Bælt.
- Moraines in Bessel Fjord (to the west of Dove Bugt) suggests that the fjord underwent multiple halts/or readvances upon deglaciation. Thus, the bathymetry of Bessel Fjord indicates that the glacial dynamics of the fjord were more dynamic than onshore evidence suggests.
- The radiocarbon date of 7.1 ~~ka~~ cal. ka BP obtained in an inner fjord core is interpreted as a minimum age at which Soranerbræen retreated to or beyond its present-day onshore position west of the fjord and is in conformity with cosmogenic nuclide dates presented by Larsen et al. (2022) in the onshore inner fjord (8.6 ka ~~cal BP~~).
- An average ~~I~~ice recession rate in Bessel Fjord was determined to be ~14 m/yr using data from this study as well as cosmogenic nuclide dates from Larsen et al., (2022) ~~occurred at a minimum average rate of ~14 m/yr~~.
- The GrIS retreated from the marine realm in the early Holocene, around the time of the onset of the HTM in this region. From this we suggest that increased Northern Hemisphere summer insolation that peaked in the early Holocene was the main control for this part of the deglaciation.
- ~~A low sedimentation rate of 13.63 cm/ka~~ Sedimentological evidence after 7.1 ~~ka~~ cal. ka BP in HH17-1289~~, and~~ (i.e., the presence of only massive mud)~~,~~ suggests that Soranerbræen did not expand back into Bessel Fjord for the remainder of the Holocene.
- The transition of mud to muddy sand at 4 ~~ka~~ cal. ka BP in a mid-fjord core HH17-1289 may provide evidence for local ice cap growth. Thus, ice caps in Bessel Fjord may have fluctuated with greater sensitivity to climatic conditions than the NE sector of the GrIS during the cooling phase that followed the HTM.

Data availability: The bathymetry and core data from UiT The Arctic University of Norway will be available upon reasonable request at UiT's open research data repository: https://dataverse.no/dataverse/uit.

Author contributions: Jan Sverre Laberg and Tom Arne Rydningen designed this study and collected the new data during the 2017 TUNU VII cruise. The bathymetrical and lithological data were interpreted by Kevin Zoller in collaboration with Jan Sverre Laberg and Tom Arne Rydningen. Kevin Zoller prepared the manuscript with contributions from all co-authors.

Competing interests: The authors declare that they have no conflict of interest.

Acknowledgement: We would like to thank the participants of the 2017 TUNU cruise to Greenland for making this project possible. A special thanks to the captain and crew of the RV *Helmer Hanssen* for their involvement in the cruise and assistance in collecting the data. A thanks also goes out to the lab staff at UiT, Trine Dahl, Karina Monsen and Ingvild Hald, who assisted with processing sediment core samples for this project. We would also like to thank Gesine Mollenhauer and the lab staff at the Alfred Wegener Institut for providing us with radiocarbon dated material using their MICADAS. Funding for this work was provided by UiT The Arctic University of Norway.

References

Arndt, J. E.: Marine geomorphological record of Ice Sheet development in East Greenland since the Last Glacial Maximum, J. Quat. Sci., 33, 853–864, https://doi.org/10.1002/jqs.3065, 2018.

Arndt, J. E., Jokat, W., Dorschel, B., Mykleburst, R., Dowdeswell, J. A., and Evans, J.: A new bathymetry of the Northeast Greenland continental shelf: Constraints on glacial and other processes, AGU Publ. Geochemistry Geophys. Geosystems, 16, 267–300, https://doi.org/10.1002/2014GC005684.Key, 2015.

Arndt, J. E., Jokat, W., and Dorschel, B.: The last glaciation and deglaciation of the Northeast Greenland continental shelf revealed by hydro-acoustic data, Quat. Sci. Rev., 160, 45–56, 2017.

Batchelor, C. L., Dowdeswell, J. A., and Rignot, E.: Submarine landforms reveal varying rates and styles of deglaciation in North-West Greenland fjords, Mar. Geol., 402, 60–80, https://doi.org/10.1016/j.margeo.2017.08.003, 2018.

Bennike, O. and Björck, S.: Chronology of the last recession of the Greenland Ice Sheet, J. Quat. Sci., 17, 211–219, https://doi.org/10.1002/jqs.670, 2002.

Bennike, O. and Weidick, A.: Late Quaternary history around Nioghalvfjerdsfjorden and Jøokelbugten, North-East Greenland, Boreas, 30, 205–227, https://doi.org/10.1111/j.1502-3885.2001.tb01223.x, 2001.

Bennike, O., Sørensen, M., Fredskild, B., Jacobsen, B. H., BöCher, J., Amsinck, S. L., Jeppesen, E., Andreasen, C., Christiansen, H. H., and Humlum, O.: Late Quaternary Environmental and Cultural Changes in the Wollaston Forland Region, Northeast Greenland, Adv. Ecol. Res., 40, 45–79, https://doi.org/10.1016/S0065-2504(07)00003-7, 2008.

Bentley, C. R.: Antarctic ice streams: a review, Geophys. Res., 92(6), 8843–8858, 1987.

Biette, M., Jomelli, V., Chenet, M., Braucher, R., Rinterknecht, V., and Lane, T.: Mountain glacier fluctuations during the Lateglacial and Holocene on Clavering Island (northeastern Greenland) from 10Be moraine dating, Boreas, 49, 873–885, https://doi.org/10.1111/bor.12460, 2020.

Björck, S. and Persson, T.: Late Weichselian and Flandrian biostratigraphy and chronology from hochstetter forland, northeast Greenland, Medd. Om. Grønl. Geosci., 5, 1–19, 1981.

Björck, S., Wohlfarth, B., Bennike, O., Hjort, C., and Persson, T.: Revision of the early Holocene lake sediment based chronology and event stratigraphy on Hochstetter Forland, NE Greenland, Boreas, 23, 513–523, https://doi.org/10.1111/j.1502-3885.1994.tb00619.x, 1994.

Boulton, G. S. and Deynoux, M.: Sedimentation in glacial environments and the identification of tills and tillites in ancient sedimentary sequences, Precambrian Res., 15, 397–422, https://doi.org/10.1016/0301-9268(81)90059-0, 1981.

Boulton, G. S., Hagdorn, M., and Hulton, N. R. J.: Streaming flow in an ice sheet through a glacial cycle, Ann. Glaciol., 36, 117–128, https://doi.org/10.3189/172756403781816293, 2003.

Briner, J. P., McKay, N. P., Axford, Y., Bennike, O., Bradley, R. S., de Vernal, A., Fisher, D., Francus, P., Fréchette, B., Gajewski, K., Jennings, A., Kaufman, D. S., Miller, G., Rouston, C., and Wagner, B.: Holocene climate change in Arctic Canada and Greenland, Quat. Sci. Rev., 147, 340–364, https://doi.org/10.1016/j.quascirev.2016.02.010, 2016.

Cartigny, M. J. B., Postma, G., Berg, J. H., and Mastbergen, D. R.: A comparative study of sediment waves and cyclic steps based on geometries, internal structures and numerical modeling, Mar. Geol., 280, 40–56, 2011.

Christiansen, J. S.: The TUNU-Programme : Euro-Arctic Marine Fishes — Diversity and Adaptation, in: Adaptation and Evolution in Marine Environments, vol. 1, 35–50, https://doi.org/10.1007/978-3-642-27352-0, 2012.

Clark, C. D.: Mega-scale lineations and cross-cutting ice-flow landforms, Earth Surf. Process. Landforms, 18, 1–29, 1993.

Clark, C. D. and Stokes, C. R.: Palaeo-ice stream landsystem, in: Glacial Landscapes, edited by: Evans, D. J. A., Edward Arnold, London, 204–227, 2003.

Clark, C. D., Tulaczyk, S. M., Stokes, C. R., and Canals, M.: A groove-ploughing theory for the production of mega-scale glacial lineations, and implications for ice-stream mechanics, J. Glaciol., 49, 240–256, https://doi.org/10.3189/172756503781830719, 2003.

Cohen, J., Screen, J. A., Furtado, J. C., Barlow, M., Whittleston, D., Coumou, D., Francis, J., Dethloff, K., Entekhabi, D., Overland, J., and Jones, J.: Recent Arctic amplification and extreme mid-latitude weather, Nat. Publ. Gr., 7, 627–637, https://doi.org/10.1038/ngeo2234, 2014.

Cremer, H., Bennike, O., and Wagner, B.: Lake sediment evidence for the last deglaciation of eastern Greenland, Quat. Sci. Rev., 27, 312–319, https://doi.org/10.1016/j.quascirev.2007.09.004, 2008.

Davies, J., Mathiasen, A. M., Kristiansen, K., Hansen, K. E., Wacker, L., Alstrup, A. K. O., Munk, O. L., Pearce, C., and Seidenkrantz, M. S.: Linkages between ocean circulation and the Northeast Greenland Ice Stream in the Early Holocene, Quat. Sci. Rev., 286, 107530, https://doi.org/10.1016/j.quascirev.2022.107530, 2022.

Dowdeswell, J. A., Ottesen, D., Evans, J., Cofaigh, C. Ó., and Anderson, J. B.: Submarine glacial landforms and rates of ice-stream collapse, Geology, 36, 819–822, https://doi.org/10.1130/G24808A.1, 2008.

Dowdeswell, J. A., Hogan, K. A., Ó Cofaigh, C., Fugelli, E. M. G., Evans, J., and Noormets, R.: Late Quaternary ice flow in a West Greenland fjord and cross-shelf trough system: submarine landforms from Rink Isbrae to Uummannaq shelf and slope, Quat. Sci. Rev., 92, 292–309, 2014.

Dowdeswell, J. A., Canals, M., Jakobsson, M., Todd, B. J., Dowdeswell, E. K., and Hogan, K. A.: The variety and distribution of submarine glacial landforms and implications for ice-sheet reconstruction, Geol. Soc. Mem., 46, 519–552, https://doi.org/10.1144/M46.183, 2016.

Evans, J., Dowdeswell, J. A., Grobe, H., Niessen, F., Stein, R., Hubberten, H. W., and

Whittington, R. J.: Late Quaternary sedimentation in Kejser Franz Joseph Fjord and the continental margin of East Greenland, Geol. Soc. Spec. Publ., 203, 149–179, https://doi.org/10.1144/GSL.SP.2002.203.01.09, 2002.

Evans, J., Ó Cofaigh, C., Dowdeswell, J. A., and Wadhams, P.: Marine geophysical evidence for former expansion and flow of the Greenland Ice Sheet across the north-east Greenland continental shelf, J. Quat. Sci., 24, 279–293, 2009.

Eyles, N., Eyles, C. H., and Niall, An. D.: Lithofacies types and vertical profile models; an alternative approach to the description and environmental interpretation of glacial diamict and diamictite sequences, Sedimentology, 30, 393–410, 1983.

Folk, R. L.: The Distinction between Grain Size and Mineral Composition in Sedimentary-Rock Nomenclature, J. Geol., 62, 344–359, 1954.

Folk, R. L. and Ward, W.: Brazos river bar, a study in the significance of grain size parameters., J. Sediment. Petrol., 27, 34–59, 1957.

Forwick, M. and Vorren, T. O.: Deglaciation history and post-glacial mass movements in Balsfjord, northern Norway, Polar Res., 21(2), 259–266, 1998.

Forwick, M., Vorren, T. O., Hald, M., Korsun, S., Roh, Y., Vogt, C., and Yoo, K. C.: Spatial and temporal influence of glaciers and rivers on the sedimentary environment in Sassenfjorden and Tempelfjorden, Spitsbergen, Geol. Soc. London, Spec. Publ., 344, 163–193, https://doi.org/10.1144/SP344.13, 2010.

Funder, S., Kjeldsen, K. K., Kjær, H. K., and Ó Cofaigh, C.: The Greenland Ice Sheet During the Past 300,000 Years: A Review, Dev. Quat. Sci., 15, 699–713, https://doi.org/10.1016/B978-0-444-53447-7.00050-7, 2011.

Funder, S., Sørensen, A. H. L., Larsen, N. K., Bjørk, A. A., Briner, J. P., Olsen, J., Schomacker, A., Levy, L. B., and Kjær, K. H.: Younger Dryas ice margin retreat in Greenland: new evidence from southwestern Greenland, Clim. Past, 17, 587–601, 2021.

Geirsdóttir, Á., Hardardóttir, J., and Andrews, J. T.: Late-Holocene terrestrial glacial history of Miki and I.C. Jacobsen Fjords, East Greenland, Holocene, 10, 123–134, https://doi.org/10.1191/095968300666213169, 2000.

Håkansson, L., Graf, A., Strasky, S., Ivy-ochs, S., Kubik, P. W., Hjort, C., Shlüchter, C., Geografiska, S., Series, A., Geography, P., Hakansson, L., Graf, A., Strasky, S., Ivy-ochs, S., Kubik, P. W., Hjort, C., and Schlichter, C.: Cosmogenic 10Be-Ages from the Store Koldewey Island, NE Greenland, Geogr. Ann. Ser. A Phys. Geogr., 89, 195–202, 2007.

Hansen, K. E., Lorenzen, J., Davies, J., Wacker, L., Pearce, C., and Seidenkrantz, M.-S.: Deglacial to Mid Holocene environmental conditions on the northeastern Greenland shelf, Quanternary Sci. Rev., 293, 107704, 2022.

Heaton, T. J., Köhler, P., Butzin, M., Bard, E., Reimer, R. W., Austin, W. E. N., Ramsey, C. B., Grootes, P. M., Hughen, K. A., Kromer, B., Reimer, P. J., and Heaton, T. J.: Marine20 — The Marine Radiocarbon Age Calibration Curve (0-55,000 CAL BP), Radio, 62, 779–820, https://doi.org/10.1017/RDC.2020.68, 2020.

Heaton, T. J., Bard, E., Ramsey, C. B., Butzin, M., Hatté, C., Hughen, K. A., Köhler, P., and Reimer, P. J.: A Response to Community Questions on the Marine20 Radiocarbon Age Calibration Curve: Marine Reservoir Ages and The Calibration of 14C Samples from the

Oceans, Radiocarbon, 65, 247–273, https://doi.org/10.1017/RDC.2022.66, 2022.

Higgins, A. K.: North Greenland Glaeier Velocities and Calf Ice Production, Polarforschung, 60, 1–23, 1991.

Hill, P. R.: Changes in submarine channel morphology and strata development from repeat multibeam surveys in the Fraser River delta, western Canada, in: Sediments, Morphology and Sedimentary Processes on Continental Shelves, edited by: Li, M. Z., Sherwood, C. R., and Hill, P. R., Blackwell Science, International Association of Sedimentologists, 47–70, 2012.

Hjort, C.: Glaciation in northern East Greenland during the Late Weichselian and Early Flandrian, Boreas, 8, 281–296, https://doi.org/10.1111/j.1502-3885.1979.tb00812.x, 1979.

Hjort, C.: A glacial chronology for northern East Greenland, Boreas, 10, 259–274, 1981.

Hjort, C. and Björck, S.: A re-evaluated glacial chronology for Northern East Greenland, Geol. Föreningen i Stock. Förhandlingar, 105, 235–243, https://doi.org/10.1080/11035898309452590, 1983.

Hogan, K. A., Dowdeswell, J. A., Noormets, R., Evans, J., and Ó Cofaigh, C.: Evidence for full-glacial flow and retreat of the Late Weichselian Ice Sheet from the waters around Kong Karls Land, eastern Svalbard, Quat. Sci. Rev., 29, 3563–3582, https://doi.org/10.1016/j.quascirev.2010.05.026, 2010.

Hogan, K. A., Ó Cofaigh, C., Jennings, A. E., Dowdeswell, J. A., and Hiemstra, J. F.: Deglaciation of a major palaeo-ice stream in Disko Trough, West Greenland, Quat. Sci. Rev., 147, 5–26, 2016.

Huddart, D. and Lister, H.: The Origin of Ice Marginal Terraces and Contact Ridges of East Kangerdluarssuk Glacier, SW Greenland, Geogr. Ann., 63 A, 31–39, 1981.

Jackson, R., Andreasen, N., Oksman, M., Andersen, T. J., Pearce, C., Seidenkrantz, M.-S., and Ribeiro, S.: Marine conditions and development of the Sirius Water polynya on the North-East Greenland shelf during the Younger Dryas-Holocene, Quat. Sci. Rev., 291, 107647, 2022.

Jakobsson, M., Hogan, K. A., Mayer, L. A., Mix, A., Jennings, A., Stoner, J., Eriksson, B., Jerram, K., Mohammad, R., Pearce, C., Reilly, B., and Stranne, C.: The Holocene retreat dynamics and stability of Petermann Glacier in northwest Greenland, Nat. Commun., 9, https://doi.org/10.1038/s41467-018-04573-2, 2018.

Jakobsson, M., Mayer, L. A., Bringensparr, C., Castro, C. F., Mohammad, R., Johnson, P., Ketter, T., Accettella, D., Amblas, D., An, L., Arndt, J. E., Canals, M., Casamor, J. L., Chauché, N., Coakley, B., Danielson, S., Demarte, M., Dickson, M. L., Dorschel, B., Dowdeswell, J. A., Dreutter, S., Fremand, A. C., Gallant, D., Hall, J. K., Hehemann, L., Hodnesdal, H., Hong, J., Ivaldi, R., Kane, E., Klaucke, I., Krawczyk, D. W., Kristoffersen, Y., Kuipers, B. R., Millan, R., Masetti, G., Morlighem, M., Noormets, R., Prescott, M. M., Rebesco, M., Rignot, E., Semiletov, I., Tate, A. J., Travaglini, P., Velicogna, I., Weatherall, P., Weinrebe, W., Willis, J. K., Wood, M., Zarayskaya, Y., Zhang, T., Zimmermann, M., and Zinglersen, K. B.: The International Bathymetric Chart of the Arctic Ocean Version 4.0, Sci. Data, 7, 1–14, https://doi.org/10.1038/s41597-020-0520-9, 2020.

Joughin, I., Fahnestock, M., MacAyeal, D., Bamber, J. L., and Gogineni, P.: Observation and analysis of ice flow in the largest Greenland ice stream, J. Geophys. Res. Atmos., 106, 34021–34034, https://doi.org/10.1029/2001JD900087, 2001.

Kelly, M. A., Lowell, T. V., Hall, B. L., Schaefer, J. M., Finkel, R. C., Goehring, B. M., Alley, R.

B., and Denton, G. H.: A 10Be chronology of lateglacial and Holocene mountain glaciation in the Scoresby Sund region, east Greenland: implications for seasonality during lateglacial time, Quat. Sci. Rev., 27, 2273–2282, 2008.

Kempf, P., Forwick, M., Laberg, J. S., and Vorren, T. O.: Late Weichselian and Holocene sedimentary palaeoenvironment and glacial activity in the high-arctic van Keulenfjorden, Spitsbergen, The Holocene, 23 (11), 1607–1618, https://doi.org/10.1177/0959683613499055, 2013.

Khan, S. A., Kjær, K. H., Bevis, M., Bamber, J. L., Wahr, J., Kjeldsen, K. K., Bjørk, A. A., Korsgaard, N. J., Stearns, L. A., Van Den Broeke, M. R., Liu, L., Larsen, N. K., and Muresan, I. S.: Sustained mass loss of the northeast Greenland ice sheet triggered by regional warming, Nat. Clim. Chang., 4, 292–299, https://doi.org/10.1038/nclimate2161, 2014.

King, E. C., Hindmarsh, R. C. A., and Stokes, C. R.: Formation of mega-scale glacial lineations observed beneath a West Antarctic ice stream, Nat. Geosci., 2, 585–588, https://doi.org/10.1038/ngeo581, 2009.

King, M. D., Howat, I. M., Candela, S. G., Noh, M. J., Jeong, S., Noël, B. P. Y., van den Broeke, M. R., Wouters, B., and Negrete, A.: Dynamic ice loss from the Greenland Ice Sheet driven by sustained glacier retreat, Commun. Earth Environ., 1, 1–7, https://doi.org/10.1038/s43247-020-0001-2, 2020.

Klages, J. P., Kuhn, G., Hillenbrand, C.-D., Graham, A. G. C., Smith, J. A., Larter, R. D., and Gohl, K.: First geomorphological record and glacial history of an inter-ice stream ridge on the West Antarctic continental shelf, Quat. Sci. Rev., 61, 47–61, 2013.

Klages, J. P., Kuhn, G., Graham, A. G. C., Hillenbrand, C.-D., Smith, J. A., Nitsche, F. O., Larter, R. D., and Gohl, K.: Palaeo-ice stream pathways and retreat style in the easternmost Amundsen Sea Embayment, West Antarctica, revealed by combined multibeam bathymetric and seismic data, Geomorphology, 245, 207–222, 2015.

Klug, M., Schmidt, S., Melles, M., Wagner, B., Bennike, O., and Heiri, O.: Lake sediments from Store Koldewey, Northeast Greenland, as archive of Late Pleistocene and Holocene climatic and environmental changes, Boreas, 38, 59–71, https://doi.org/10.1111/j.1502-3885.2008.00038.x, 2009a.

Klug, M., Bennike, O., and Wagner, B.: Repeated short-term bioproductivity changes in a coastal lake on Store Koldewey, northeast Greenland: An indicator of varying sea-ice coverage?, Holocene, 19, 653–663, https://doi.org/10.1177/0959683609104040, 2009b.

Klug, M., Bennike, O., and Wagner, B.: Late Pleistocene to early Holocene environmental changes on Store Koldewey, coastal north-east Greenland, Polar Res., 35, https://doi.org/10.3402/polar.v35.21912, 2016.

Kobashi, T., Menviel, L., Jeltsch-Thömmes, A., Vinther, B. M., Box, J. E., Muscheler, R., Nakaegawa, T., Pfister, P. L., Döring, M., Leuenberger, M., Wanner, H., and Ohmura, A.: Volcanic influence on centennial to millennial Holocene Greenland temperature change, Sci. Rep., 7, 1–10, https://doi.org/10.1038/s41598-017-01451-7, 2017.

Kolling, H. M., Stein, R., Fahl, K., Perner, K., and Moros, M.: Short-term variability in late Holocene sea ice cover on the East Greenland Shelf and its driving mechanisms, Palaeogeogr. Palaeoclimatol. Palaeoecol., 485, 336–350, https://doi.org/10.1016/j.palaeo.2017.06.024, 2017.

Krieger, L., Floricioiu, D., and Neckel, N.: Drainage basin delineation for outlet glaciers of

Northeast Greenland based on Sentinel-1 ice velocities and TanDEM-X elevations, Remote Sens. Environ., 237, 111483, https://doi.org/10.1016/j.rse.2019.111483, 2020.

Laberg, J. S., Forwick, M., and Husum, K.: New geophysical evidence for a revised maximum position of part of the NE sector of the Greenland ice sheet during the last glacial maximum, Arktos, 3, https://doi.org/10.1007/s41063-017-0029-4, 2017.

Lambeck, K., Rouby, H., Purcell, A., Sun, Y., and Sambridge, M.: Sea level and global ice volumes from the Last Glacial Maximum to the Holocene, Proc. Natl. Acad. Sci., 111, 15296–15303, https://doi.org/10.1073/pnas.1411762111, 2014.

Landvik, J. Y.: The last glaciation of Germania Land and adjacent areas, northeast Greenland, J. Quat. Sci., 9, 81–92, https://doi.org/10.1002/jqs.3390090108, 1994.

Lane, T. P., Roberts, D. H., Ó Cofaigh, C., Vieli, A., and Moreton, S. G.: The glacial history of the southern Svartenhuk Halvø, West Greenland, Arktos, 1, 1–28, https://doi.org/10.1007/s41063-015-0017-5, 2015.

Larsen, N. K., Funder, S., Linge, H., Möller, P., Schomacker, A., Fabel, D., Xu, S., and Kjær, K. H.: A Younger Dryas re-advance of local glaciers in north Greenland, Quat. Sci. Rev., 147, 47–58, https://doi.org/10.1016/j.quascirev.2015.10.036, 2016.

Larsen, N. K., Levy, L. B., Carlson, A. E., Buizert, C., Olsen, J., Strunk, A., Bjørk, A. A., and Skov, D. S.: Instability of the Northeast Greenland Ice Stream over the last 45,000 years, Nat. Commun., 9, 3–10, https://doi.org/10.1038/s41467-018-04312-7, 2018.

Larsen, N. K., Søndergaard, A. S., Levy, L. B., Olsen, J., Strunk, A., Bjørk, A. A., and Skov, D.: Contrasting modes of deglaciation between fjords and inter-fjord areas in eastern North Greenland, Boreas, 49, 905–919, https://doi.org/10.1111/bor.12475, 2020.

Larsen, N. K., Søndergaard, A. S., Levy, L. B., Strunk, A., Skov, D. S., Bjørk, A., Khan, S. A., and Olsen, J.: Late glacial and Holocene glaciation history of North and Northeast Greenland, Arctic, Antarct. Alp. Res., 54, 294–313, https://doi.org/10.1080/15230430.2022.2094607, 2022.

Levy, L. B., Kelly, M. A., Lowell, T. V., Hall, B. L., Howley, J. A., and Smith, C. A.: Coeval fluctuations of the Greenland ice sheet and a local glacier, central East Greenland, during late glacial and early Holocene time, Geophys. Res. Lett., 43, 1623–1631, 2016.

Lyså, A. and Vorren, T. O.: Seismic facies and architecture of ice-contact submarine fans in high-relief fjords, Troms, Northern Norway, Boreas, 26, 309–328, 1997.

Mouginot, J., Rignot, E., Scheuchl, B., Fenty, I., Khazendar, A., Morlighem, M., Buzzi, A., and Paden, J.: Fast retreat of Zachariae Isstrom, Northeast Greenland, Science (80-.)., 350, 1357–1361, 2015.

Mouginot, J., Bjørk, A. A., Millan, R., Scheuchl, B., and Rignot, E.: Insights on the Surge Behavior of Storstrømmen and L. Bistrup Bræ, Northeast Greenland, Over the Last Century, Geophys. Res. Lett., 45, 11,197-11,205, https://doi.org/10.1029/2018GL079052, 2018.

Newton, A. M. W., Knutz, P. C., Huuse, M., Gannon, P., Brocklehurst, S. H., Clausen, O. R., and Gong, Y.: Ice stream reorganization and glacial retreat on the northwest Greenland shelf, Geophys. Res. Lett., 44, 7826–7835, https://doi.org/10.1002/2017GL073690, 2017.

Ó Cofaigh, C.: Flow Dynamics and till genesis associated with a marin-based Antarctic palaeo-ice stream, Quat. Sci. Rev., 24, 709–740, 2005.

Ó Cofaigh, C., Dowdeswell, J. A., and Grobe, H.: Holocene glacimarine sedimentation, inner Scoresby Sund, East Greenland: The influence of fast-flowing ice-sheet outlet glaciers, Mar. Geol., 175, 103–129, https://doi.org/10.1016/S0025-3227(01)00117-7, 2001.

Ó Cofaigh, C., Dowdeswell, J. A., Jennings, A. E., Hogan, K. A., Kilfeather, A., Hiemstra, J. F., Noormets, R., Evans, J., McCarthy, D. J., Andrews, J. T., Lloyd, J. M., and Moros, M.: An extensive and dynamic ice sheet on the west greenland shelf during the last glacial cycle, Geology, 41, 219–222, https://doi.org/10.1130/G33759.1, 2013.

Olsen, I. L., Forwick, M., Laberg, J. S., and Rydningen, T. A.: Last Glacial ice-sheet dynamics offshore NE Greenland – a case study from Store Koldewey Trough, The Cryosphere Discussions, 2020.

Ottesen, D., Dowdeswell, J. A., and Rise, L.: Submarine landforms and the reconstruction of fast-flowing ice streams within a large Quaternary ice sheet: The 2500-km-long Norwegian-Svalbard margin (57°-80°N), Bull. Geol. Soc. Am., 117, 1033–1050, https://doi.org/10.1130/B25577.1, 2005.

Ottesen, D., Dowdeswell, J. A., Benn, D. I., Kristensen, L., Christiansen, H. H., Christensen, O., Hansen, L., Lebesbye, E., Forwick, M., and Vorren, T. O.: Submarine landforms characteristic of glacier surges in two spitsbergen fjords, Quat. Sci. Rev., 27, 1583–1599, 2008.

Pados-Dibattista, T., Pearce, C., Detlef, H., Bendtsen, J., and Seidenkrantz, M. S.: Holocene palaeoceanography of the Northeast Greenland shelf, Clim. Past, 18, 103–127, https://doi.org/10.5194/cp-18-103-2022, 2022.

Pedersen, J. B. T., Kroon, A., and Jakobsen, B. H.: Holocene sea-level reconstruction in the Young Sound region, Northeast Greenland, J. Quat. Sci., 26(2), 219–226, 2011.

Rahmstorf, S., Box, J. E., Feulner, G., Mann, M. E., Robinson, A., Rutherford, S., and Schaffernicht, E. J.: Exceptional twentieth-century slowdown in Atlantic Ocean overturning circulation, Nat. Clim. Chang., 5, 475–480, https://doi.org/10.1038/nclimate2554, 2015.

Reeh, N., Bøggild, C. E., and Oerter, H.: Surge of Storstrømmen, a large outlet glacier from the Inland Ice of North-East Greenland, Rapp. Grønands Geol. Unders., 162, 201–209, 1994.

Reilly, B. T., Stoner, J. S., Mix, A. C., Walczak, M. H., Jennings, A., Jakobsson, M., Dyke, L., Glueder, A., Nicholls, K., Hogan, K. A., Mayer, L. A., Hatfield, Robert, G., Albert, S., Marcott, S., Fallon, S., and Cheseby, M.: Holocene break-up and reestablishment of the Petermann Ice Tongue, Northwest Greenland, Quat. Sci. Rev., 218, 322–342, 2019.

Reimer, P. J., Austin, W. E. N., Bard, E., Bayliss, A., Blackwell, P. G., Bronk Ramsey, C., Butzin, M., Cheng, H., Edwards, R. L., Friedrich, M., Grootes, P. M., Guilderson, T. P., Hajdas, I., Heaton, T. J., Hogg, A. G., Hughen, K. A., Kromer, B., Manning, S. W., Muscheler, R., Palmer, J. G., Pearson, C., Van Der Plicht, J., Reimer, R. W., Richards, D. A., Scott, E. M., Southon, J. R., Turney, C. S. M., Wacker, L., Adolphi, F., Büntgen, U., Capano, M., Fahrni, S. M., Fogtmann-Schulz, A., Friedrich, R., Köhler, P., Kudsk, S., Miyake, F., Olsen, J., Reinig, F., Sakamoto, M., Sookdeo, A., and Talamo, S.: The IntCal20 Northern Hemisphere Radiocarbon Age Calibration Curve (0-55 cal kBP), Radiocarbon, 62, 725–757, https://doi.org/10.1017/RDC.2020.41, 2020.

Rignot, E., Bjork, A., Chauche, N., and Klaucke, I.: Storstrømmen and L. Bistrup Bræ, North Greenland, Protected From Warm Atlantic Ocean Waters, Geophys. Res. Lett., 49, https://doi.org/10.1029/2021GL097320, 2022.

Rydningen, T. A., Vorren, T. O., Laberg, J. S., and Kolstad, V.: The marine-based NW Fennoscandian ice sheet: Glacial and deglacial dynamics as reconstructed from submarine landforms, Quat. Sci. Rev., 68, 126–141, https://doi.org/10.1016/j.quascirev.2013.02.013, 2013.

Sættem, J.: Glaciotectonic forms and structures on the Norwegian continental shelf: observations, processes and implications, Nor. Geol. Tidsskr., 70, 81–94, 1990.

Schaffer, J., von Appen, W.-J., Dodd, P. A., Hofstede, C., Mayer, C., de Steur, L., and Kanzow, T.: Warm water pathways toward Nioghalvfjerdsfjorden Glacier, Northeast Greenland, J. Geophys. Res. Ocean., 122, 4004–4020, https://doi.org/10.1002/2016JC012462.Received, 2017.

Schmidt, S., Wagner, B., Heiri, O., Klug, M., Bennike, O., and Melles, M.: Chironomids as indicators of the Holocene climatic and environmental history of two lakes in Northeast Greenland, Boreas, 40, 116–130, https://doi.org/10.1111/j.1502-3885.2010.00173.x, 2011.

Schoof, C. G. and Clarke, G. K. C.: A model for spiral flows in basal ice and the formation of subglacial flutes based on a Reiner-Rivlin rheology for glacial ice, J. Geophys. Res. Solid Earth, 113, 1–12, https://doi.org/10.1029/2007JB004957, 2008.

Shaw, J., Pugin, A., and Young, R. R.: A meltwater origin for Antarctic shelf bedforms with special attention to megalineations, Geomorphology, 102, 364–375, https://doi.org/10.1016/j.geomorph.2008.04.005, 2008.

Shreve, R. L.: Esker characteristics in terms of glacier physics, Katahdin esker system, Maine., Geol. Soc. Am. Bull., 96, 639–646, https://doi.org/10.1130/0016-7606(1985)96<639:ECITOG>2.0.CO;2, 1985.

Skov, D. S., Andersen, J. L., Olsen, J., Jacobsen, B. H., Knudsen, M. F., Jansen, J. D., Larsen, N. K., and Egholm, D. L.: Constraints from cosmogenic nuclides on the glaciation and erosion history of Dove Bugt , northeast Greenland, GSA Bull., 1–13, 2020.

Slabon, P., Dorschel, B., Jokat, W., Myklebust, R., Hebbeln, D., and Gebhardt, C.: Greenland ice sheet retreat history in the northeast Baffin Bay based on high-resolution bathymetry, Quat. Sci. Rev., 154, 182–198, https://doi.org/10.1016/j.quascirev.2016.10.022, 2016.

Smith, L. M. and Andrews, J. T.: Sediment characteristics in iceberg dominated fjords, Kangerlussuaq region, East Greenland, Sediment. Geol., 130, 11–25, https://doi.org/10.1016/S0037-0738(99)00088-3, 2000.

Stacey, C. D. and Hill, P. R.: Cyclic steps on a glacifluvial delta, Howe Sound, British Columbia, in: Atlas of Submarine Glacial Landforms: Modern, Quaternary and Ancient, edited by: Dowdeswell, J. A., Canals, M., Jakobsson, M., Todd, B. J., Dowdeswell, E. K. & Hogan, K. A., Geological Society of London, 93–94, 2016.

Stocker, T. F., Qin, D., Plattner, G.-K., Tignor, M. M. B., Allen, S. K., Boschung, J., Nauels, A., Xia, Y., Bex, V., and Midgley, P. M.: Climate Change 2013: The Physical Science Basis. Contribution of Working Group I to the Fifth Assessment Report of the Intergovernmental Panel on Climate Change, Cambridge, 2013.

Stokes, C. R. and Clark, C. D.: Geomorphological criteria for identifying Pleistocene ice streams, Ann. Glaciol., 28, 67–74, https://doi.org/10.3189/172756499781821625, 1999.

Stokes, C. R. and Clark, C. D.: Palaeo-ice streams, Quat. Sci. Rev., 20, 1437–1457, 2001.

Storrar, R. D., Stokes, C. R., and Evans, D. J. A.: Morphometry and pattern of a large sample

(>20,000) of Canadian eskers and implications for subglacial drainage beneath ice sheets, Quat. Sci. Rev., 105, 1–25, https://doi.org/10.1016/j.quascirev.2014.09.013, 2014.

Syring, N., Lloyd, J. M., Stein, R., Fahl, K., Roberts, D. H., Callard, L., and O'Cofaigh, C.: Holocene interactions between glacier retreat, sea ice formation, and Atlantic water advection at the inner Northeast Greenland continental shelf, Paleoceanogr. Paleoclimatology, 35, 2020.

Wagner, B., Bennike, O., Bos, J. A. A., Cremer, H., Lotter, A. F., and Melles, M.: A multidisciplinary study of Holocene sediment records from Hjort Sø on Store Koldewey, Northeast Greenland, J. Paleolimnol., 39, 381–398, https://doi.org/10.1007/s10933-007-9120-3, 2008.

Weber, M. E., Niessen, F., Kuhn, G., and Wiedicke, M.: Calibration and application of marine sedimentary physical properties using a mult-sensor core logger, Mar. Geol., 136, 151–172, 1997.

Weidick, A., Andreasen, C., Oerter, H., and Reeh, N.: Neoglacial glacier changes around Storstrommen, north-east Greenland, Polarforschung, 64, 95–108, 1994.

Wilson, N. J. and Straneo, F.: Water exchange between the continental shelf and the cavity beneath Nioghalvfjerdsbræ (79 North Glacier), Geophys. Res. Lett., 42, 7648–7654, https://doi.org/10.1002/2015GL064944, 2015.

Winkelmann, D., Jokat, W., Jensen, L., and Schenke, H. W.: Submarine end moraines on the continental shelf off NE Greenland - Implications for Lateglacial dynamics, Quat. Sci. Rev., 29, 1069–1077, https://doi.org/10.1016/j.quascirev.2010.02.002, 2010.